JOINT EUROPEAN TORUS

JET–P(89)05

K. Behringer, B. Denne, M. Forrest, M. Stamp, H.P. Summers
and JET Team

Spectroscopic Determination of Impurity Influx from Localised Surfaces

Spectroscopic Determination of Impurity Influx from Localised Surfaces

K. Behringer, B. Denne, M. Forrest, M. Stamp, H.P. Summers
and JET Team*

JET-Joint Undertaking, Culham Science Centre, OX14 3DB, Abingdon, UK

** See Appendix 1*

Preprint of Paper to be submitted for publication in
Journal in Physics B

ABSTRACT

The flux of impurity atoms into plasmas from limiting surfaces is considered. It is shown how the flux of an impurity released from a surface can be derived from spectroscopic measurements along a line-of-sight directed at the surface. A theoretical atomic level population model is developed to obtain the "ionisation per emitted photon" quantities which link the spectroscopic measurement to the flux. Metastable states and finite density plasma effects are taken into account and observations at visible wavelengths are emphasised. Detailed studies and calculations are performed for C^{+1}, C^{+2}, O^{+1}, O^{+2}, Cr, Cr^{+1}, Fe, Fe^{+1}, Ni and Ni^{+1}. Tabulations and graphs of relevant quantities are provided. The application of the theory to impurity influxes in the JET tokamak is described.

1. INTRODUCTION

In fusion plasmas, ions of the commonly occurring impurity elements such as carbon, oxygen, chromium, iron and nickel can radiate strongly in virtually all temperature and density environments and excitation conditions. All these environments and the behaviour of impurities in them are therefore accessible to study spectroscopically. For contained thermonuclear fusion devices such as JET, two environments are of special importance, namely the near equilibrium, high temperature central plasma and the low temperature highly non-equilibrium edge plasma. In the latter, the plasma approaches and interacts significantly with its bounding walls and limiters. The material inflow under this interaction is an important parameter. This paper is concerned with spectroscopic measurements of the impurity composition of this material inflow and the quantifying of the inward fluxes.

The broad picture is fairly simple. The principal influxes occur from sputtering of surfaces which the plasma contacts. In JET these are limiters, inner wall protection tiles and radio frequency antennae protection plates. The plasma in the immediate vicinity of such a surface has electron thermal energy large compared with the ionisation potentials of atoms leaving the surface. Ionisation of the impurity atoms therefore occurs very rapidly through several ionisation stages before the atom has diffused significantly into the plasma volume. In the course of this ionisation, each ionisation stage radiates and this can be measured spectroscopically along a line of sight directed at the sputtering surface. Atoms in higher ionisation stages penetrate further into the plasma and disperse as they are entrained in the motion of the plasma as a whole. The low stages of ionisation tend to be well localised and the higher stages less so. Measurements of the radiation from low stages of impurities can therefore be converted fairly easily into fluxes of impurities from the surfaces. Because the localised radiation is from low stages of ionisation,

suitable spectrum lines for observation generally fall in visible and quartz UV spectral regions. This is of observational convenience and is emphasised in this paper.

Theoretical analysis relates line of sight integrals of spectral line emission to ionisation stage abundances and then to impurity fluxes. A complication is added by the highly ionising conditions. Most impurity ionisation stages of interest have low lying metastable levels which are significantly populated as well as the ground level in the inflowing material. The relaxation time of metastable populations to equilibrium with the associated ground population at the plasma electron temperature is of the order of or larger than the ionisation time. The metastable populations are therefore not uniquely determined from knowledge of the ground population but dependent also upon how they are 'born' from the previous stage. The initial distribution of metastable populations of neutral atoms on leaving a sputtering surface is not clearly known nor are the atomic ionisation rates creating a metastable ion from a metastable neutral and so on. The spectroscopic measurements for fluxes must therefore make independent determination of metastable and ground populations.

In section 2, the overall theoretical diffusion model is examined in some generality. The atomic models required for the practical implementation of this are considered in Section 3. Detailed application to ions of carbon, oxygen, chromium, iron and nickel is described in Section 4. Tables and figures allowing application to the interpretation of arbitrary plasmas are given. Results in application to JET are given in Section 5 and the concluding remarks are in Section 6.

2. PHYSICAL MODEL

2.1 Fluxes

Suppose the boundary sputtering surface is the plane $\zeta=0$, and the spectroscopic line of sight is the -ve ζ direction. We are concerned with fluxes from the surface in the +ve ζ direction. It is convenient to adopt a Cartesian coordinate frame. For JET, ionisation lengths are small compared with minor section curvature so it is simplest to combine cylindrical effects with the lateral spreading into a single term perpendicular to the ζ direction.

Consider then an impurity element A. Denote the z-times ionised ion in the σ^{th} metastable state by A_σ^{+z} and the corresponding population number density at position ζ by $n_\sigma(z,\zeta)$. Let the flux of ions A_σ^{+z} be $\Gamma_\sigma(z,\zeta)$. The impurity transport number balance for ions A_σ^{+z} is

$$\frac{\partial}{\partial t} n_\sigma(z,\zeta) + \frac{\partial}{\partial \zeta} \Gamma_\sigma(z,\zeta) + \underline{\nabla}_\perp \cdot \underline{\Gamma}_\sigma(z,\zeta)$$

$$= \sum_{\sigma''} N_e \, S_{\sigma''\to\sigma}(z-1,z) \, n_{\sigma''}(z-1,\zeta)$$

$$-\Big\{\sum_{\sigma''} N_e \, S_{\sigma\to\sigma'}(z,z+1)\Big\} n_\sigma(z,\zeta) + \sum_{\rho} N_e \, \not{C}_{\rho\to\sigma}(z,z) n_\rho(z,\zeta)$$

$$-\Big\{\sum_{\rho} N_e \, \not{C}_{\sigma\to\rho}(z,z)\Big\} \, n_\sigma(z,\zeta) \qquad (1)$$

Recombination is neglected and we assume each stage is connected only with the adjacent stages. The sum σ' is over metastables of stage z+1 and the sum σ'' is over metastables of stage z-1. $S_{\sigma''\to\sigma}(z-1,z)$ denotes the effective ionisation rate from metastable σ'' of stage z-1 to metastable σ of stage z. $\not{C}_{\rho\to\sigma}(z,z)$ denotes the collisonal-radiative coefficient from metastable ρ of stage z to metastable σ of stage z. By definition, it is the composite effective rate coefficient taking account of collisional and radiative processes by both direct and indirect paths from ρ to σ. N_e is the electron

density. For simplicity in the equations, we have omitted positive ion collisions without loss of generality. It is convenient to define also

$$\begin{aligned} \phi_\sigma(z,z) &= \sum_\rho \phi_{\sigma\to\rho}(z,z) \\ S_\sigma(z,z+1) &= \sum_{\sigma'} S_{\sigma\to\sigma'}(z,z+1) \\ n(z,\zeta) &= \sum_\sigma n_\sigma(z,\zeta) \\ \Gamma(z,\zeta) &= \sum_\sigma \Gamma_\sigma(z,\zeta) \end{aligned} \tag{2}$$

Summing over metastables of stage z gives

$$\begin{aligned} \frac{\partial}{\partial t} n(z,\zeta) + \frac{\partial}{\partial \zeta} \Gamma(z,\zeta) + \underline{\nabla}_\perp \cdot \underline{\Gamma}(z,\zeta) \\ = \sum_{\sigma,\sigma''} N_e S_{\sigma''\to\sigma}(z-1,\zeta) n_{\sigma''}(z-1,\zeta) \\ - \sum_{\sigma,\sigma'} N_e S_{\sigma\to\sigma'}(z,z+1)\, n_\sigma(z,\zeta) \end{aligned} \tag{3}$$

Also sum from stages z=o to Z

$$\begin{aligned} \frac{\partial}{\partial t} \sum_{z=o}^{Z} n(z,\zeta) + \frac{\partial}{\partial \zeta} \sum_{z=o}^{Z} \Gamma(z,\zeta) + \underline{\nabla}_\perp \cdot \sum_{z=o}^{Z} \underline{\Gamma}(z,\zeta) \\ = - \sum_{\sigma,\sigma'} N_e S_{\sigma\to\sigma'}\, n_\sigma(Z,\zeta) \end{aligned} \tag{4}$$

Assume a steady state is reached and integrate from $\zeta=0^+$ to ∞. (The integral is from just outside the sputtering surface.)

$$\begin{aligned} \sum_{z=o}^{Z} \Gamma(z,\infty) - \sum_{z=o}^{Z} \Gamma(z,o) = - \int_o^\infty \sum_o N_e S_\sigma(Z,Z+1) n_\sigma(Z,\zeta)\, d\zeta \\ - \int_o^\infty \underline{\nabla}_\perp \cdot \sum_{z=o}^{Z} \underline{\Gamma}(z,\zeta)\, d\zeta \end{aligned} \tag{5}$$

If Z is chosen sufficiently small so that all the impurity

ions ultimately ionize beyond stage Z, then $\sum_{z=o}^{Z} \Gamma(z,\infty)=o$

Separating the flux orthogonal to the surface into inward (away from the surface) Γ^{in} and outward (towards the surface) Γ^{out} parts at the surface,

$$\sum_{z=o}^{Z} \Gamma^{in}(z,o) = \int_o^\infty \sum_\sigma N_e S_\sigma (Z,Z+1)\, n_\sigma(Z,\zeta)d\zeta + D(Z) + \sum_{z=o}^{Z} \Gamma^{out}(z,o) \qquad (6)$$

where D(Z) is a transverse dispersive flux loss and $\sum_{z=o}^{Z} \Gamma^{out}(z,o)$ is a return loss to the surface. For low states of ionisation therefore such that the lateral dispersion and return losses may be neglected, the inward flux along the line of sight up to stages Z from the boundary surface is related to an integral over the abundances of the metastables of the stage Z alone. Provided no ions emerge from the sputtering surface in ionisation stages above Z, this is just the overall inward impurity flux Γ^A. That is

$$\Gamma^A = \sum_{z=o}^{Z} \Gamma^{in}(z,o) = \int_o^\infty N_e \sum_\sigma S_\sigma(Z,Z+1) n_\sigma(Z,\zeta)d\zeta \qquad (7)$$

Evidently

$$\begin{aligned} &\int_o^\infty \underline{\nabla}_\perp \cdot \{\underline{\Gamma}(Z+1,\zeta) - \underline{\Gamma}(Z,\zeta)\}d\zeta + \Gamma^{out}(Z+1,o) \\ &\qquad = \int_o^\infty N_e \sum_{\sigma'} S_{\sigma'}(Z+1,Z+2) n_{\sigma'}(z+1,\zeta)d\zeta \\ &\qquad - \int_o^\infty N_e \sum_\sigma S_\sigma(Z,Z+1) n_\sigma(Z,\zeta)d\zeta \end{aligned} \qquad (8)$$

is a measure of the lateral dispersion flux and return losses of stage Z+1. If the terms on the right hand side were precisely known, then this formula could be used to give the

lateral dispersion flux in higher ionisation stages. Formula 7 may be used for all stages which do not experience significant dispersion and return losses. It presupposes no knowledge of the collisional radiative coefficients $\not{C}_{\rho\to\sigma}(z,z)$ coupling metastables of the same stage together. Also it should be noted that the total effective ionisation rate out of a metastable σ, $S_\sigma(z,z+1)$ is much more accurately known that the components $S_{\sigma\to\sigma'}(z,z+1)$.

2.2 Intensities

Excited level populations of an ionisation stage are relaxed relative to the ground and metastable level populations at all timescales of relevance here.

(a) **Low density** The equilibrium is between collisional excitation and radiative decay. Consider excited level i of ionisation stage Z and suppose this is excited only from the metastable level σ.

therefore, omitting the coordinate ζ in expressions

$$\sum_{\substack{k \\ k<i}} A_{i\to k}\, n_i(Z) = Ne\; q_{\sigma\to i}\; (1+c_{\sigma,i})\; n_\sigma(Z) \qquad (9)$$

where the A's are Einstein coefficients, q's excitation rate coefficients by electrons and c's are cascade corrections. The emissivity in the transition i→j is

$$\varepsilon_{\sigma,i\to j} = A_{i\to j}\, n_i(Z) = \left(\frac{A_{i\to j}}{\sum_k A_{i\to k}}\right) Ne\; q_{\sigma\to i}(1+c_{\sigma,i}) n_\sigma(Z) \qquad (10)$$

The subscript σ in $\varepsilon_{\sigma,i\to j}$ indicates that this emissivity is dependent on the population of the metastable level σ. Substituting in 7, the flux is

$$\Gamma^A = \int_o^\infty \sum_\sigma \left(\frac{\sum_k A_{i\to k}}{A_{i\to j}}\right)\left(\frac{S_\sigma(Z,Z+1)}{q_{\sigma\to i}}\right)\left(\frac{1}{1+c_{\sigma,i}}\right)\varepsilon_{\sigma,i\to j}\, d\zeta \qquad (11)$$

If the plasma temperature and density are approximately constant in the vicinity of the ionising shell of stage Z then

$$\Gamma^{A} = \sum_{\sigma} \left\{ \left(\frac{\sum_{k} A_{i\to k}}{A_{i\to j}} \right) \left(\frac{S_{\sigma}(Z,Z+1)}{q_{\sigma\to i}} \right) \left(\frac{1}{(1+c_{\sigma,i})} \right) \right\} I_{\sigma,i\to j} \qquad (12)$$

where $I_{\sigma,i\to j} = \int_{0}^{\infty} \varepsilon_{\sigma,i\to j}\, d\zeta$ is the line of sight emissivity.

(b) **High density and metastable mixing** At high density, equation 8 is incorrect since the equilibrium must include collisional redistribution processes amongst the excited levels. Also an excited level population may be dependent on more than one metastable level. These processes are described in general by the collisional-radiative matrix. The elements are

$$C_{ki} = \begin{cases} -\frac{1}{Ne} A_{i\to k} - q_{i\to k} & (k<i) \\ -q_{i\to k} & (k>i) \end{cases} \qquad (13)$$

$$C_{ii} = \frac{1}{Ne} \sum_{k<i} A_{i\to k} + \sum_{k=i} q_{i\to k} + S_{i}$$

where S_i is the ionisation rate coefficient. Then the excited level population equations become

$$\sum_{i} Ne\, C_{ki}\, n_{i}(Z) = Ne \sum_{\sigma} C_{k\sigma}\, n_{\sigma}(Z) \qquad (14)$$

so that

$$n_{i}(Z) = \sum_{k} C^{-1}_{ik} \sum_{\sigma} C_{k\sigma}\, n_{\sigma}(Z) \qquad (15)$$

The emissivity of spectrum line i→j is then

$$\varepsilon_{i\to j} = A_{i\to j} \sum_{k} C^{-1}_{ik} \sum_{\sigma} C_{k\sigma}\, n_{\sigma}(Z) \qquad (16)$$

To solve for $n_{\sigma}(Z)$, we used a linearly independent set of

lines of the same number as the number of metastables. Labelling these lines by the index ρ, then if the emissivity of the ρ^{th} line arises from the $i \to j$ transition from $n_i(Z)$ then

$$\varepsilon_\rho \equiv \varepsilon_{\rho, i\to j} = A_{i\to j} \sum_k C^{-1}_{ik} \sum_\sigma C_{k\sigma}\, n_\sigma(Z)$$

or symbolically

$$\varepsilon_\rho = \sum_\sigma W_{\rho\sigma}\, n_\sigma(Z) \qquad (17)$$

$W_{\rho\sigma}$ is non-singular so that

$$n_\sigma(Z) = \sum_\rho W^{-1}_{\sigma\rho}\, \varepsilon_\rho$$

and the flux becomes

$$\Gamma^A = \sum_{\sigma,\rho} \{N_e\, S_\sigma\,(Z,Z+1)\, W^{-1}_{\sigma\rho}\} I_\rho \qquad (18)$$

with $I_\rho = \int_0^\infty \varepsilon_\rho\, d\zeta$ in analogy with the earlier result (equation 12).

Evidently even at low density, parent mixing can cause a composite contribution to the population of an excited level (cf. the right hand side of equation 14) and so lead to a similar form 18, even though only radiative terms occur in the collisional radiative matrix C_{ki}.

2.3 Evolution of metastable populations

It is evident from the previous section that to derive the flux from the emission of an ionisation stage with a certain number of significantly populated metastables, an equal number of spectrum lines must be measured. Only a weighted sum of the separate metastable abundances is used in the final total flux derivation. The component abundances allow

comment on ionisation rate coefficients from metastable to metastable and/or the temperature in the vicinity of the sputtering surface. We adopt a simplified model in which the plasma temperature and density are assumed constant at all relevant distances from the sputtering surface and suppose that the impurity ions have a fixed velocity v in the ζ direction. Neglecting lateral dispersion and using partitioned matrix notation, the set of equations 1, for all stages up to Z become

$$\frac{d}{d\tau}\begin{bmatrix}\underline{n}(0)\\ \underline{n}(1)\\ \vdots\\ \underline{n}(Z)\end{bmatrix} = \begin{bmatrix}\underline{\underline{C}}(0,0) & & & \\ \underline{\underline{C}}(1,0) & \underline{\underline{C}}(1,1) & & \\ & \ddots & \ddots & \\ & & \underline{\underline{C}}(Z,Z-1) & \underline{\underline{C}}(Z,Z)\end{bmatrix}\begin{bmatrix}\underline{n}(0)\\ \underline{n}(1)\\ \vdots\\ \underline{n}(Z)\end{bmatrix} + \begin{bmatrix}-\underline{\underline{S}}(0,1) & & & \\ \underline{\underline{S}}(0,1) & -\underline{\underline{S}}(1,2) & & \\ & \ddots & \ddots & \\ & & \underline{\underline{S}}(Z-1,Z) & 0\end{bmatrix}\begin{bmatrix}\underline{n}(0)\\ \underline{n}(1)\\ \vdots\\ \underline{n}(Z)\end{bmatrix} \qquad (19)$$

where $\tau = \frac{N_e \zeta}{v}$. If the electron temperature is sufficiently high, the second term dominates the first. Metastable populations are then 'frozen' as they were created from the stage before. If the first term is comparable with or smaller than the second, excitation of a metastable of a stage from the ground state of that stage can occur. Domination by the first term establishes the usual statistical balance picture adopted in most circumstances near equilibrium.

Let the diagonal matrix of eigenvalues be diag $\{\lambda^{(1)}, \ldots, \lambda^{(m)}\}$ and the corresponding full matrix of eigenvectors be $\underline{\underline{U}}$. Then the population distribution at ζ=o can be reconstructed from the observed line emissivities and the submatrices $\underline{\underline{W}}$ (see equation 17). These are

$$\begin{bmatrix} \underline{n}(0) \\ \underline{n}(1) \\ \\ \underline{n}(7) \end{bmatrix}_{J=0} = \frac{N_e}{v} \underline{\underline{U}}\, \mathrm{diag}\left\{\lambda^{(1)} \ldots \lambda^{(m)}\right\} \underline{\underline{U}}' \begin{bmatrix} \underline{\underline{W}}^{-1}(0) & & \\ & & \\ & & \underline{\underline{W}}^{-1}(7) \end{bmatrix} \begin{bmatrix} \underline{I}(0) \\ \underline{I}(1) \\ \underline{I}(7) \end{bmatrix} \qquad (20)$$

The distribution may be unrealistic if the assumed temperature is incorrect, or there are errors in the rate coefficients. Some consistency of the assumed parameters may then be pursued. The direct ionisation rates ratiod to one of them and the electron temperature seem the logical parameters to vary to ensure an initial distribution resembling expectations. The primary reason for a differential variation in the ionisation coefficient ratios would be incorrect assumptions about the inner shell/auto-ionisation contributions. This is an important area to probe. Note that the solution is independent of v and only weakly dependent on the electron density at least at moderate and low densities.

3. ATOMIC MODELS

To evaluate the quantities identified in section 2 requires a large amount of basic atomic data. Much of this data is not available. It has been necessary therefore to make a number of supplementary ab initio calculations. In this section we outline the methods used. The impurities to be addressed include the light elements carbon and oxygen (ion stages C^{+}, C^{+2}, O^{+}, O^{+2}) and the metals chromium, iron and nickel (ion stages Cr^{+0}, Cr^{+1}, Fe^{+0}. Fe^{+1}. Ni^{+0}, Ni^{+1}). That is we are concerned with ionisation and excitation of ions in ground and metastable configurations of the form $2s^{q_1}2p^{q_2}$ in the first case and of the form $3d^{q_1}4s^{q_2}$ in the second. The corresponding radiative transitions of importance are of the form $2s^{q_1}2p^{q_2-1}3\ell - 2s^{q_1}2p^{q_2-1}3\ell'$ in the light elements and of the forms $3d^{q_1}4s^{q_2} - 3d^{q_1}4s^{q_2-1}4p$ and $3d^{q_1}4s^{q_2} - 3d^{q_1-1}4s^{q_2}4p$ in the metals.

3.1 Ionisation rate coefficients

The reaction is

$$A_{\sigma}^{+z} + e \rightarrow A_{\sigma'}^{+z+1} + e + e \qquad (21)$$

where σ denotes a metastable term of stage z and σ' a metastable term of stage z+1. Let the direct electron collisional ionisation rate coefficient for a Maxwellian electron distribution of temperature Te from a hypothetical state γ of ionisation potential I_γ and occupation number (number of equivalent electrons) ζ_γ be described by $q^{(i)}(\zeta_\gamma, I_\gamma)$. Simple semi-empirical formulae for ionisation express this as

$$q^{(i)}(\zeta_\gamma, I_\gamma) = 2.1715\times10^{-8}\ C\ \omega\ \zeta_\gamma \left(\frac{I_H}{kTe}\right)^{\frac{1}{2}} \left(\frac{I_H}{I_\gamma}\right) E_1\left(\frac{I_\gamma}{kTe}\right) \qquad (22)$$

where E_1 is the first exponential integral. ω is a factor introduced to give some empirical improvement for very low stages of ionisation, particularly neutral ionisation. It is

equal to unity for ionisation from higher stages. The factor ω approaches unity as I_γ/kTe becomes small. This is the situation of relevance here. C is an overall scaling factor. Burgess & Chidichimo (1982) suggest C=2.3. The Lotz (1967) value for C is 2.77. Our objective is to construct partial ionisation rates from ground and metastable terms of one ionisation stage to the ground and metastable terms of the next ionisation stage. Excitation/autoionisation must be taken into account. Since the Maxwellian electron temperature is of the order of the ionisation potentials in our circumstances, the threshold region of the cross-section is of relatively less importance for the rate coefficients. Also the rates are likely to be less sensitive to the finite threshold steps of excitation/autoionisation. Radiative stabilisation of autoionising resonances may be neglected for the low stages of ionisation here. We propose therefore that all rate coefficients for light ions can be constructed from linear combinations of the basic formula 22 with suitable choices of ζ_γ and I_γ and some speculation on spin and parent weighting. That is any ionization rate $S(z,z+1)_{\sigma\to\sigma'}$ may be written as

$$S(z,z+1)_{\sigma\to\sigma'} = \sum_\gamma \alpha_\gamma \, q^{(i)}(\zeta_\gamma, I_\gamma) \qquad (23)$$

where the coefficients α_γ, ζ_γ and I_γ are deduced from the ionisation pathways involved. We ignore collisional-radiative ionisation via bound excited levels since the electron densities here are barely sufficient for the stepwise processes and these are further reduced by the large (kT_e/I_γ) value. The inherent uncertainty in the empirical formulae does not warrant greater elaboration.

We illustrate the derivation of the parameters α_γ, ζ_γ, I_γ with an example of ionisation of a boron-like ion in the ground state $2s^2 2p\ ^2P$ leaving a residual beryllium-like ion either in the $2s^2\ ^1S$ ground state or the $2s2p\ ^3P$ metastable state. The principal thresholds are shown in the energy diagram.

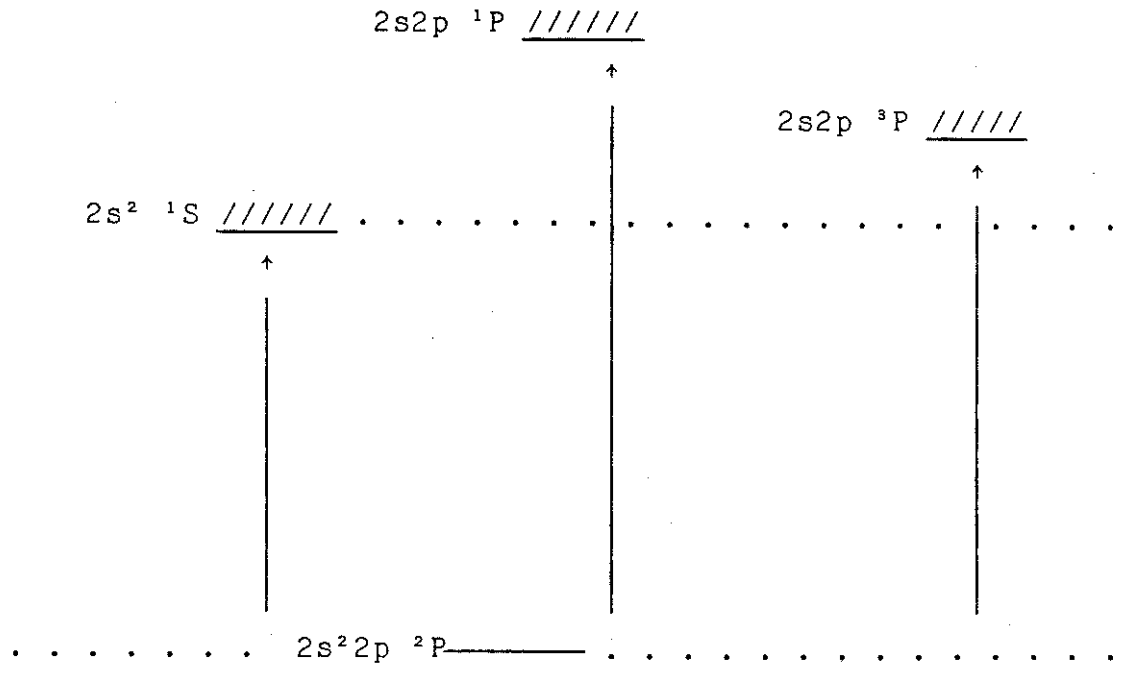

The ionisation rate coefficient leaving the residual ion in the state $2s^2\ ^1S$ is

$$S(2s^22p\ ^2P \rightarrow 2s^2\ ^1S) = q^{(i)}(1,I_1) + \tfrac{1}{4}\, q^{(i)}(2,I_1) + \tfrac{3}{4}\,[q^{(i)}(2,I_1) - q^{(i)}(2,I_2)] \qquad (24)$$

The first term is the direct 2p loss. The second term is the 2s loss to the singlet side. This introduces a factor ¼. Singlet levels between I_1 and I_3 autoionise to $2s^2\ ^1S+e$ with unit probability. Levels above I_3 radiate leading to $2s^2\ ^1S$. Therefore all singlet levels above I_1 contribute to $2s^2\ ^1S$. The third term is 2s loss to the triplet side. This introduces a factor ¾. Levels between I_1 and I_2 autoionise to $2s^2\ ^1S+e$ with unit probability.

The ionisation rate coefficient leaving the $2s2p\ ^3P$ residual ion is

$$S(2s^22p\ ^2P \rightarrow 2s2p\ ^3P) = \tfrac{3}{4}\, q^{(i)}(2,I_2) \qquad (25)$$

The ionisation rate coefficient for $2s^2 2p\ ^2P$ without resolution of final state is

$$S(2s^2 2p\ ^2P) = q^{(i)}(1,I_1) + q^{(i)}(2,I_1) = q^{(i)}(3,I_1) \quad (26)$$

consistent with the prescription of Burgess et al (1978).

Table 1a shows the α_γ, ζ_γ and I_γ values adopted for all light ions under consideration here.

For ionisation of the metallic ions Cr^{+1}, Fe^{+1}, Ni^{+1}, experimental cross-section data is available (Man et al., 1987; Montague et al., 1984; Montague & Harrison, 1985). These 'cross-beam' results indicate that the use of semi-empirical formulae (Burgess & Chidichimo, 1983; Lotz, 1969) is unreliable leading to quite substantial overestimation of the cross-sections. This is with standard assignments of shell occupancies and thresholds. The experimental data however does not distinguish unambiguously the initial ionising state, since the ion beams have unknown metastable fractions. On the other hand, it might be expected that the separate ionisation cross-sections from ground and metastables will converge to a universal curve at reasonably high electron energies ($\gtrsim$ 2 x threshold). This is due to the strong weighting of the cross-section by inner shell electron ionisation. We have represented the ionisation cross-section from metastables at low energy by straight lines from the appropriate thresholds tangent to the experimental curve and at high energy by the experimental curve. Maxwellian averaged rate coefficients were calculated by direct numerical quadrature of the cross-sections. In view of our arbitrary treatment of the threshold region, we anticipate that there may be significant errors in our rates at temperatures < 10-20 eV. There is no reliable experimental data for ionisation of Cr^{+0}, Fe^{+0}, Ni^{+0}. Comparison of the theoretical calculation of McGuire (1977) with the cross-beam for the ions data (see eq. Man et al., 1987) shows that for energies $\gtrsim$ 50 eV, the theoretical data

is usually lower, at most 40%, than the experimental (the largest deviation is for Cr^{+1}) but generally closer. We have chosen to use the McGuire calculation for Cr^{+0}, Fe^{+0}, Ni^{+0}. We have no confident assessment of error in these cases, but on the basis of the above remarks anticipate some underestimation of the true ionisation rates. The same procedure for the metastable threshold regions is used as for the ions. Table 1b shows the metastables and thresholds adopted for the metallic ions.

3.2 Excitation rates

The excitation rate data required for this work is more extensive than that needed for measurements on resonance lines in the VUV. For the light elements, the main visible spectral lines for observation correspond to n=3-3 transitions. For the lines to be observable, the primary excitation to the excited level from the ground or metastable level must be forbidden so that there is no subsequent strong radiative branch via an n=3-2 resonance line. Cross-section data is often not available especially for n=2-3 non dipole excitations in the light elements and there is virtually no collision data for low ionisation stages of transition metals. In consequence, we have found it necessary to calculate some of our own data. We have available a number of collision codes for this including distorted wave and close coupling techniques. There is, however, again the helpful simplification that the electron thermal energies are high. The collisional rates are therefore not strongly dependent on the near threshold part of the collision strengths, which is most markedly disturbed by resonances. The reactance matrix elements are not sensitive to the accuracy of the free waves. For JET with relevant plasma temperatures $\gtrsim$ 50 eV, the accurate collision strengths are substantially converged to the Born asymptotic forms. For this reason we have prepared a Born approximation described in section 3.2.1. The accuracy of the target is of greater importance. We describe the target states used in our Born calculations also in section 3.2.1. In Section 3.3 our more elaborate target investigations required especially for the transition metals are described.

3.2.1 Effective potential Born approximation collision strengths

The reaction is

$$A_{\gamma}^{+z} + e(E) \rightarrow A_{\gamma'}^{+z} + e(E')$$

E and E' are the initial and final electron energies with E > E' and $\Delta E = E - E'$ is the transition energy. The Born collision strength takes the usual form

$$\Omega_{\gamma\gamma'}(E,E') = \omega_\gamma \, 8 \sqrt{\frac{EE'}{I_H}} \sum_\lambda Q^{(\lambda)}_{\gamma\gamma'} R^{(\lambda)}(E,E') \qquad (27)$$

where the sum is over the various multipoles λ. $Q^{(\lambda)}_{\gamma\gamma'}$ comprises the angular factors and $R^{(\lambda)}$ the momentum and radial integrals. The Ochkur extension allows the application to spin change transitions, but with different $Q^{(\lambda)}_{\gamma\gamma'}$ and $R^{(\lambda)}$'s. (cf Vainshtein & Sobelman, 1967).

Case (a) no spin change $\gamma = (SpLp)n\ell SL \quad ; \gamma' = (SpLp)n\ell' SL'$

$$Q^{(\lambda)}_{\gamma\gamma'} = (2\ell+1)(2\ell'+1)(2L'+1)(2\lambda+1) \begin{Bmatrix} \ell & L & Lp \\ L' & \ell' & \lambda \end{Bmatrix}^2 \begin{pmatrix} \ell & \ell' & \lambda \\ 0 & 0 & 0 \end{pmatrix}^2 \qquad (28)$$

$$R^{(\lambda)}(E,E') = \int_{-1}^{1} \frac{\left| \langle n\ell \left| j_\lambda(qr) \right| n'\ell' \rangle \right|^2}{\alpha_0^4 q^4} \, d(\cos\theta) \qquad (29)$$

Case (b) spin change $\gamma = (SpLp)n\ell SL \quad ; \gamma' = (SpLp)n\ell' S'L'$

$$Q^{(\lambda)}_{\gamma\gamma'} = \frac{(2S'+1)}{2(2Sp+1)} (2\ell+1)(2\ell'+1)(2L'+1)(2\lambda+1) \begin{Bmatrix} \ell & L & Lp \\ L' & \ell' & \lambda \end{Bmatrix}^2 \begin{pmatrix} \ell & \ell' & \lambda \\ 0 & 0 & 0 \end{pmatrix}^2 \qquad (30)$$

$$R^{(\lambda)}(E,E') = \int_{-1}^{1} \frac{\left| \langle n\ell \left| j_\lambda(qr) \right| n'\ell' \rangle \right|^2}{a_0^4 q^4} \left(\frac{q}{k}\right)^4 d(\cos\theta) \qquad (31)$$

q is the momentum transfer at scattering angle Θ and k is the initial momentum. Other notation is conventional. The radial integrals are evaluated from numerical wave functions. We adopt a parametrised effective central potential as the basis for calculating these wave functions. The central potential is established by defining an effective screening configuration

$$n_1\ell_1^{\,q_1}\ n_2\ell_2^{\,q_2}\ \ldots\ n_s\ell_s^{\,q_s}$$

such that $q_1 + q_2 + \ldots + q_s = z_o - z_1$ where z_o is the nuclear charge and $z_1 = z+1$. The electron in shell i is supposed to be screened from the nucleus by the electrons in shells <i and partially screened by the other electrons in shell i itself. So the effective charge for i^{th} shell electrons is

$$z_i = z_o - \sum_{j=1}^{i-1} q_j - \tfrac{1}{2}q_i \qquad (32)$$

The adopted (Slater type) potential is then

$$V(r) = \frac{z_o}{r} - \sum_{i=1}^{s} \frac{q_i}{r}\, e^{-\alpha_i z_i r/n_i}\, r^{ni}\Big(\sum_{k=o}^{n_i} a_{ik} r^{-k}\Big) \qquad (33)$$

The α_i are adjustable parameters chosen so that the one-electron wave function satisfies the one-electron Schrodinger equation with potential V(r) and the observed eigenvalue ε and quantum defect μ. In practice, we set $\alpha_i = \overline{\alpha}_i\ \alpha$ with $\overline{\alpha}_i$ specified so that only the overall scaling parameter α is varied to match the observed quantum defect. The $\overline{\alpha}_i$ follow from more general optimising of the potential. The radial integrals are evaluated by numerical quadruture.

We have imposed a finite threshold in the collision strengths for positive ions by a displacment of the incident energy. This follows the prescription of Cowan (1981).

3.2.2 Impact parameter collision strengths

For redistributive collisions between levels of excited principal quantum shells only dipole transitions induced by positive ions and electrons need to be considered. For these we use the semi classical impact parameter theory Burgess (1964) as described in detail by Burgess and Summers (1976). Transitions between ground term fine structure components are

induced primarily by positive ion impact and are of electric quadrupole type. We have available the semi classical impact parameter theory of Bely (unpublished), (see also Gordon et al 1983) for such transitions. Trial calculations for JET indicate that fine structure populations of a ground or metastable term are full collisionally mixed. They therefore have statistical relative populations. In these circumstances only term populations need to be considered in our further calculations. On JET, observed multiplet components with pure upper states indicate relative statistical populations for ground and metastable state fine structure levels.

3.3 Structure calculations

We have used the multielectron multiconfiguration structure code SUPERSTRUCTURE (Eissner et al 1974) to calculate some unknown oscillator strengths in light ions. Precise oscillator strengths are also needed for many transitions in metallic ions. Investigations on $Ni^{+\circ}$ indicated that ab initio calculation with SUPERSTRUCTURE could not improve on semi-empirical methods (eg Kurucz & Peytremann, 1975).

4. GENERAL RESULTS

4.1 Light Elements

4.1.1 Sources of atomic data

The energy diagram for C^{+1} is given in Figure 1. This shows the complete set of terms included in our calculations together with the mean multiplet wavelengths and adopted dipole A-values. The A-values have been taken primarily from Weise et al (1966). A recent calculation is available for the n=2-3 transitions from the ground term and the n=3-3 transitions with (^{1}S) parent. The difference with Weise et al is less than 15% in all cases. We have calculated A-values for $2s2p^2\ ^4P$ - $2s2p(^3P)3s\ ^4P$, $2s2p^2\ ^2P$-$2s^23p\ ^2P$ and $2s2p^2\ ^2D$ - $2s^23p\ ^2P$ with SUPERSTRUCTURE. These were not given by Weise et al. Nine configurations were used but low confidence must be placed in the '2-electron jump' estimates. This will also be true for the $2s2p^2\ ^2S$ - $2s^23p\ ^2P$ transition in Weise et al. These transitions do unfortunately provide a significant loss pathway from $3p\ ^2P$. Collision strengths are taken from Robb (Magee et al 1977) within the n=2 complexes and for $2s^22p^2P$ - $2s^23s$, $2s^23p\ ^2P$ and $2s^23d\ ^2D$ from Mann (Magee et al 1977) (see also Itikawa et al 1983). All other n=2-3 and 3-3 collision strengths have been calculated following the methods of Section 3.2.

The energy diagram for C^{+2} is given in Figure 2. This beryllium-like ion has been extensively studied. Recent A-value data is available from Fawcett (1984) which we have adopted here. Agreement is fairly good with the older work of Glass (1979), the largest differences being for 3-3 transitions (up to 30%). New collision strength data has been published by Berrington et al (1976) for transitions within the n=2 complexes. As for C^{+1}, Coulomb-Born-Exchange data of Mann (Magee et al 1977) is available for $2s^2\ ^1S$ - $2s3s\ ^1S$, $2s3p\ ^1P$ and $2s3d\ ^1D$ together with the spin changing transitions. We adopt this data and use the methods of Section 3.2 for all other transitions. Note that spin change collision rates are not of great importance here since the lowest ground or metastable of each spin system tends to be

significantly populated. Direct excitations therefore dominate.

The energy diagram for O^{+1} is given in Figure 3. A-values have been taken from Weise et al and are shown in the figure. Collision strengths within the ground configuration $2s^22p^3$ are taken from Henry et al (1969). Ho and Henry (1983) also provide the $2s^22p^3\ ^4S$ - $2s2p^4\ ^4P$ and $2s^22p^3\ ^4S$ - $2s^22p^2(^3P)3s\ ^4P$ collision strengths. All other data has been calculated following Section 3.2, except for the important $2s^22p^3\ ^4S$ - $2s^22p^2(^3P)3p\ ^4P$. This is an excluded Born multipole. We have performed a two-state R-matrix close coupling calculation for this transition. It does indeed show pure exchange character and is small. Some data is available from Ganas (1981) but this does not have the resolution required for the present studies.

The energy diagram for O^{+2} is given in Figure 4. Our main A-value data is taken from Weise et al. Smith and Weise (1971) have deduced improved values for some transitions from isoelectronic sequence extrapolation. We have substituted these values when available. There are some omitted transitions of the form 3p-3d. We have calculated these using SUPERSTRUCTURE. The primary collision strength data within the n=2 configurations is taken from Baluja et al (1981), supplemented with data from Mann (1981) (see Itikawa et al (1983)). All n=2-3 and 3-3 excitations are calculated with the methods of Section 3.2

The broad accuracy expectation of our Born collision strengths is ~ 40% at energies $\gtrsim$ 30 eV. This has been derived from comparisons with distorted wave data in Ne^{+6} and from comparisons with the data of Mann. The error increases at low energy somewhat unpredictably in that for most transitions accuracy is good at all energies while for a few errors up to a factor 2-3 appear at threshold. This low energy regime is not of importance for JET.

Some adjustment of the raw excitation rate data is necessary to allow for cascade from higher levels. This is specifically cascades of the form nd→3p ($n \geq 4$) in the cases where the ground or metastable excitations to 3p are forbidden and to nd are dipole allowed. We estimate these corrections by including only $4 \leq n \leq 6$, projecting the 3d term excitation collision strengths to higher n with an assumed $1/n^3$ behaviour, and using hydrogenic radial integrals in the branching A-values. It is important in this context that '2-electron jump' transitions out of the 3p levels are included in the population equations since they tend to counter the effect of the higher level cascades.

4.1.2 Spectrum lines and theoretical results

In Table 2, the important metastables (and ground levels) of C^{+1}, C^{+2}, O^{+1} and O^{+2} are indexed. Table 2 also provides a list of spectrum lines suitable for observation and derivation of metastable fluxes. The choice has been principally governed by requiring lines in the visible and quartz UV regions, by requiring them to be reasonably strong and by requiring the excitation rate coefficient to the upper level of the transition to have no marked peculiarities. By the latter we mean to exclude forbidden Born multipoles etc. This selection is convenient for tokamak observation. It is not a restriction of our methods or data base, results can equally well be provided for any of the lines shown in Figures 1 to 4. Figure 5a,b gives curves of ionisations/emitted photon as a function of temperature for the selected lines. These are results at low density and give the quantity in { } brackets in equation 12. Note that the electron temperature dependence is quite significant. The use of these results therefore requires a reasonable knowledge of the temperature in the immediate vicinity of the sputtering surface. Figure 5c shows the theoretical limits of line ratios in O^{+1} and O^{+2}, dependent on more than one metastable.

Figure 6 illustrates the full calculation of the excited level population structure at finite densities. For a specified metastable σ, the curves are of the factors on the right hand side of equation 15 divided by $N_e n_\sigma$. Figure 6 gives the dependence of the populations of O^+ on electron density and on one metastable (the ground level) at a single electron temperature. The onset of collisional redistribution amongst the excited levels is evident as the density increases. Tokamaks evidently lie in the low density regime.

Tables 3a, 3b, 3c and 3d provide the main results. The quantity in { } brackets in equation 18 is tabulated for the various ions, lines and metastables at a range of temperature

and densities. The indexing follows the specification in Table 2.

4.2 Metals

Because of the very complex energy level structure of the neutral and singly ionised ions of Cr, Fe and Ni, a full analysis comparable with that for light elements is impossible at present. For the ions Cr^{+0}, Cr^{+1}, Fe^{+0}. Fe^{+1}. Ni^{+0} and Ni^{+1} the lowest terms belong to the three forms $3d^q$, $3d^{q-1}(SpLp)4s$ and $3d^{q-2}(Sp'Lp')4s^2$, although which provides the ground term varies from ion to ion as does the ordering. In general there is a large number of parents (SpLp) and grandparents (Sp'Lp'), but the lowest of each is usually quite well separated from the others in energy. Parentage and grandparentage provide meaningful quantum numbers, although there is substantial parentage mixing. We assume that the lowest metastable of each type (including both spin systems of the second type) may be significantly populated. Since there is often an overlap in energy between the lowest metastable of one type and the higher metastables of another type, for example $3d^6(^3H)4s\ ^4H$, ^2H and $3d^5(^4S)4s^2\ ^4S$ in Fe^{+1}, we consider also the possibility of higher metastables being populated. The broad expectation however is that the higher a metastable lies above the ground, the more its population becomes neglectable.

Figure 7a, 7b, 8a, 8b, 9a and 9b give the simplified term structure for Cr^{+0}, Cr^{+1}, Fe^{+0}, Fe^{+1}, Ni^{+0} and Ni^{+1} respectively. they show the lowest metastables as described above, together with some of the principal excited terms which radiatively decay to the metastables and associated with the same parentage and grandparentage. The intensities of the multiplets shown are expected to be characteristic of the metastable term upon which they terminate. Some confusion is caused by the $3d^q$ terms. When they are low lying and when there is more than one term belonging to the configuration, as for Cr^{+1} and Fe^{+1}, the second metastable of the configuration has also been marked. Radiative decay to these metastables occurs from terms of the form $3d^{q-1}(SpLp)4p$ and hence intensities may be characteristic of a combination of the $3d^q$ and $3d^{q-1}(SpLp)4s$ metastables.

It should be noted that these are all resonance transitions. This is the principal simplification over Section 4.1 for light elements where transitions between excited levels had to be considered, and it is this which makes a low density analysis possible here. Most of the spectrum lines indicated lie in the visible and quartz UV although some have wavelengths down to 1700Å.

4.2.1 Sources of atomic data

Basic atomic data for the metastables and transitions used in the analysis are presented in tables 4a and 4b. Table 4a lists the metastables under consideration for each ion. For Cr^{+0} and Fe^{+0}, the $3d^6$ ^5D and $3d^8$ ^3F metastables respectively are high lying and are ignored. Table 4b lists the spectrum lines suggested for observation and the metastables on which they depend. The A-value column gives the spontaneous coefficient for the upper level to the corresponding metastable term. This is the relevant quantity for deriving the excitation rate coefficient to the upper level with the assumption of statistical relative populations of J levels of the metastable terms. The branching ratio is for the particular multiplet component indicated.

For Cr^{+0}, A-values are taken from Younger et al (1978). The transition from the upper level of highest J is taken in each case since these are the strongest components and have the highest purity (Roth, 1980). The branching ratios are $\geq$ 0.86 in all cases indicating that the lines are predominantly characteristic of the specified metastable. Recent precision A-values for the first and second transitions (Blackwell, 1984) differ by less than 2% from the values used here. For Cr^{+1}, the α transition can be produced following excitation from metastable 1 ($3d^5$ ^6S) or 5 ($3d^4(^5D$ $4s$ ^6D). The A-values are obtained from the compilation of Kurucz & Peytremann (1975), hereafter called KP. All the states have high purity (>83%) and one comparative A value (ie $3d^4(^5D)4p$ $^6P_{7/2}$ - $3d^4(^5D)4s$ $^6D_{5/2}$) is available from Younger et al. This is 40% greater than the KP value. The branching for the α line is quite unfavourable. It is unlikely that the $3d^5$ ^6S

population can be determined reliably. The situation is similar for the β line, although the upper level has low purity (65%) in this case. For multiplet 1, Roth indicates 100% purity for all upper and lower levels. Thus the line components might be expected to follow standard LS multiplet splitting (White and Eliason, 1933). The available components from Younger et al do not follow this. A short portion of a limiter spectrum taken during a JET pulse is shown in figure 10. This supports the White-Eliason proportions. We have inferred the A-value for the 11/2-9/2 component from White & Eliason (ie 1.41^{8} sec^{-1}) and compared it with the KP value (2.76^{8} sec^{-1}). This is within expected uncertainties and we have adopted the KP value. The levels involved in multiplet 4 also have high purity. The required component inferred from available Younger et al data and White-Eliason splitting is within 14% of KP. The branching ratio is 0.83 arising primarily from transitions to the $3d^5$ ^5G metastable. The A-value for multiplet 14 shows good agreement between inferred and KP values. For multiplet 25, there is come branching to $3d^5$ ^2H and $3d^5$ ^2I.

For Fe^{+0}, the basic A-value data is from Fuhr et al (1981). The $^3G_5$ upper level (multiplet 59) has 61% purity. This arises from spin system breakdown giving a strong branch to metastable 2. The component of multiplet 216 has a very unfavourable branching ratio. The other branches are to higher metastables (which are not separately isolated in our treatment). We cannot expect a reliable determination of metastable 5 from this line. For Fe^{+1}, A-value data for multiplets α and ν are from the calculation of Nussbaumer et al (1981), and for all other multiplets from KP. For multiplet 32, the component 11/2-9/2 gives good agreement between KP and Fuhr et al (within 26%). The low branching ratio for the Υ and δ multiplets makes confident determination of $3d^7$ ^4F and $3d^7$ ^2G metastable populations unlikely.

For Ni^{+0}, the basic data for multiplets 22, 38 and 70 are from Fuhr et at (1981). For multiplet α, the A-value of

2.3^7 sec^{-1} is from KP. Our SUPERSTRUCTURE test calculation (see section 3.3) gives 3.3^7 sec^{-1}. The branching A-value to metastable 3 is from Fuhr et al and agrees exactly with our SUPERSTRUCTURE calculation. The unfavourable branch makes $3d^{10}$ metastable population determination difficult. For Ni^{+1}, A-value data for multiplets α, β, γ, δ are from KP and for multiplets 2 and 10 from Fuhr et al. As in other cases, the branching ratio for multiplet α again is unfavourable for $3d^9$ ^2D determination.

Wavelengths above 2000Å are in air.

There are no available refined collision calculations for the ions and energy regimes here. The three simple approximate techniques which can be used are $\bar{g}$ (Van Regemorter 1962), impact parameter (Section 3.2.2) and effective potential Born (Section 3.2.1). Note that all required transitions are dipole allowed. Our SUPERSTRUCTURE calculation on $Ni^{+\circ}$, together with the work of Nussbaumer & Storey (1981), indicate that the one electron orbitals resulting from a statistical model or Slater type potential do not provide a good representation for the 3d, 4s and 4p orbitals of the neutral and singly ionised transition metals. This is shown by the necessity of including large numbers of correlation terms and the strong mixing of $3d^{q-1}4\ell$, $3d^{q-1}5\ell$ and $3d^{q-1}6\ell$ configurations. Consequently the effective potential Born treatment might be expected to be unreliable. $\bar{g}$ and impact parameter on the other hand can use the observed oscillator strength. Note again that the high energy regime is most important here where the collision strength becomes asymptotically proportional to the line strength. Impact parameter is our preferred method. Overall the accuracy expectation of the collision rates is not large and certainly somewhat less than that of the radiative transition probability data.

The theoretical results on ionisation/photon are presented in Figures 11a, 11b, 12a, 12b, 13a, 13b. Each curve is labelled by the transition wavelength and the metastable flux to which it relates (see table 4b). For ions where some lines are excited from more than one metastable, the order of analysis must be from pure lines (dependent on a single metastable) to multiple metastable dependent lines.

5. APPLICATION TO JET INFLUX MEASUREMENTS

Plasma ion (H,D,He) and impurity influxes have been measured routinely on JET by means of visible spectroscopy, viewing carbon limiters, chromium or nickel antenna screens and parts of the vacuum vessel walls. Occasionally, the JET VUV survey spectrometer has been employed for the same purpose, when

plasmas were limited by the inner wall carbon protection tiles, and therefore, plasma-wall interaction occurred in its field of view. A description of these diagnostics and further references can be found in Behringer (1986), Morgan et al. (1985), Behringer et al. (1986). Visible spectrometers and filter-photomultiplier combinations were coupled to the torus by means of ≈100 m long optical fibres, restricting the accessible wavelength range to ≈4000-7000 A. The spectrometers were equipped with optical multi-channel analysers (OMA). During earlier JET operation periods, a close-coupled monochromator was installed, viewing one of the JET poloidal limiters through a sapphire window, thus extending the wavelength range down to 2000 A in the UV. For survey purposes,its wavelength was scanned during the long flat-top phases of JET plasmas pulses. The VUV instrument covered the wavelength range between 100 and 1100 A and was absolutely calibrated by means of branching ratios and by recording predictable intensities of charge-exchange populated line transitions (Behringer et al., 1986).

Influx measurements have been carried out for determining particle confinement times, for localising important impurity sources in the tokamak, and for investigating impurity production mechanisms and production rates as a function of plasma parameters. Implications for plasma performance have already been presented in a number of publications (see eg. Behringer et al., 1985, 1987; Stamp et al., 1987; Behringer, 1988; Stamp et al., 1988), and only a few examples will be given here to illustrate the method. Hydrogen or deuterium fluxes have been routinely derived from H_α/D_α or other Balmer lines, using the well-known Johnson-Hinnov (1973) calculations. In the VUV wave-length range, L_β has served the same purpose. When dealing with helium plasmas, the flux in the He I ground state has been derived from the intensity of the He I $2p^1P_1$-$3d^1D_2$ transition at 6678 A, and the flux in the metastable level from the He I $2p^3P$-$3d^3D$ multiplet at 5876 A, using the same methods as presented in this paper. It was found that the metastable

flux is only 0.2% of the ground state and can be safely ignored (Stamp et al., 1988), not a surprising result considering its high excitation energy and the short lifetime of the He atoms in the plasma. Results, concerning impurity influxes into deuterium and helium plasmas, which are reported in the following, have always been related to the respective influxes of plasma ions, in order to draw conclusions on production yields and on the resulting impurity contamination of the respective plasmas (see Behringer, 1987 for the correlation of impurity influxes and impurity concentrations).

5.1 Light Impurity Influxes

The most comprehensive study of carbon and oxygen limiter fluxes in deuterium has been carried out during a sequence of JET pulses with 2.5 MA plasma current and a line average density $n_e \approx 2.10^{19}$ m^{-3}. An example of the visible spectra used in this analysis is given in fig.14, showing the spectral range around D_α with C II lines at 6678 and 6682 A. During the same experimental campaign, small plasmas (minor radius 0.8 m instead of 1.2 m) were produced both on the outer limiters and on the inner wall. In these cases, the plasma current was reduced to 1 MA and the electron density to 1.10^{19} m^{-3}. The VUV spectra, recorded by the survey spectrometer during these discharges, were analysed with respect to impurity release from the inner wall and the poloidal spreading of different impurity ionisation stages (Behringer et al., 1985). The inner-wall spectra are substantially different from the limiter spectra, because intensities of lines from low ionisation stages, which are representative for the localised influxes, are significantly enhanced, as demonstrated in fig.15. From the above measurements, complete sets of metastable state populations have been derived for C II, C III, O II and O III ions using the atomic data presented in this paper. The results are summarised in Tables 5 and 6. Because of the low electron densities, the analysis is very insensitive to errors in n_e. However, a reasonable knowledge of the relevant electron temperature is required. It could

only be estimated to be about 100 eV at the location of ionisation.

Tables 5 and 6 demonstrates that, with the possible exception of C II, metastable state populations can be quite significant in these ions. The results are reasonable in the sense that more particles are found in the levels with lower excitation energy or higher statistical weights. Taking into account all contributions, the agreement between results from C II and C III, and from O II and O III is very satisfactory. The metastable state population in C II, measured by visible spectroscopy, is nicely confirmed by the VUV data, while there is some discrepancy in C III. The most likely explanation here is an underestimate of the ground state from C III at 5696 A. The total carbon influxes from limiter or inner wall are also very much the same, which is probably due to similar plasma edge parameters. A production yield of order 8% can be explained by deuterium sputtering, production by oxygen and self-sputtering of carbon at low electron densities, ie. high edge temperatures (Behringer, 1987). The oxygen fluxes from the two locations are probably quite unrelated and, unfortunately, other O II and O III lines in the VUV spectra are too weak to be analysed. The total flux has, therefore, been scaled from the observed transition using the results from visible spectroscopy. The carbon-to-oxygen influx ratios of 3-4 are in very good agreement with results for the plasma interior obtained from C VI and O VIII line intensities by means of an impurity transport code, or from charge-exchange recombination spectroscopy.

Although in general the relationship of line intensities and influxes is a fairly sensitive function of electron temperature, in many cases this dependence is the same for different ions, and therefore, influx ratios are simply given by the relative brightnesses. This argument already holds for the carbon-to-oxygen ratio from Tables 5 and 6 which should be more accurate than their relation to deuterium. Also, the temperature dependences of Helium flux measurements from He I

6678 A and of carbon from C II 6578 A are very similar, allowing a measurement of the carbon production yield by helium bombardment from the two line intensities without knowing the electron temperature. An example of such measurements is shown in Fig. 16 as a function of time during a JET plasma pulse with ion cyclotron heating (ICRH) (Stamp et al., 1988). During the early phases of this pulse, when the electron density is low, a production yield of 10% is found, which later-on drops to ~ 5% in agreement with models for physical sputtering and respective changes of edge temperature. Apparently, the carbon production is not increased during ICRH.

5.2 Fluxes of Metal Impurities

Measurements of metal influxes in JET are by far less complete than light impurity results. Many of the lines in Table 4b have been observed occasionally, but the most important ground state transitions in Cr II, Fe I, Fe II, Ni I and Ni II are outside the fibre transmission range and even at the lower end of the close-coupled spectrometer wavelength range. Furthermore a survey of limiter spectra based on different plasma pulses is unreliable in this case because of the strongly varying metal coverage of the carbon tiles. Thus, only the Cr I 4254 A line has been monitored routinely from the limiters and the quintet line at 5208 A has been measured on occasion. The chromium influxes for a strongly metal-coated limiter case are given in Table 7, demonstrating the small population of the ^5S state. In general no discrepancies have been encountered when assuming the 4254 A transition to be representative for the total neutral chromium influx. Production rates of order 2%, extrapolated to a 100% metal surface, were measured in good agreement with expectations from basic sputtering data.

Important conclusion on the release of metal impurities during ICRH could be drawn from measurements of chromium influxes from a Cr coated ICRH antenna (Behringer et al., 1987a). It was found that these fluxes were roughly propor-

tional to the ICRH power supplied to this particular antenna and amounted to some 10^{19} particles/s per MW. In the course of ICRH operation, screen material was deposited on the limiters and subsequently eroded again by the plasma. The resulting balance of these production and migration processes as a function of ICRH history is shown in Fig.17 by means of the pulse-to-pulse variation of the chromium influxes from the limiter.

In the case of nickel, which is the most prominent metal impurity in JET, there are only indications from singlet lines, like the 3619 A transition, that metastable states could be significantly populated. Iron has only been seen on a few rare occasions in JET and not received further attention.

6. CONCLUDING REMARKS

The ionisation/photon predictions of this paper can be used for determination of impurity fluxes from localised surfaces over a wide range of plasma temperature. However, a large amount of atomic data has been used in obtaining these predictions, which is of uncertain reliability. We expect errors $\lesssim$ factor 2 in both ionisation and excitation rates separately, improving at higher temperatures and worsening at lower temperatures. Also, deductions of relative fluxes might be expected to be more reliable than absolute fluxes. The light element data have received some corroborative support from JET studies, but the metal data remains as largely unverified theoretical predictions. The study described here has motivated new calculations of important collision cross-sections and further experimental measurements in plasmas. Also, the same techniques will in the future be applied to beryllium in JET. From these developments, it is anticipated that refinements and extensions to the present work will be published in due course.

The spectrum lines identified for measurement in deducing metal influxes have been dictated by theoretical consideration of state purity, high J weighting and visible/quartz UV wavelengths. Line blending may make the measurements impossible in certain cases. The multiplet spreads are quite large and so it is probable in such circumstances that alternative members of the multiplet will be suitable. Because of state mixing, conversion of the ionisation/photon results to a different member may not be immediate. Some data is available on alternative members on request from the authors.

The possibility of charge transfer from neutral hydrogen contributing to the observed spectrum line emissions has been ignored. It is clear that charge transfer from thermal neutral hydrogen at the plasma periphery in JET can modify emission (cf. the Lyman series of C VI (Mattioli et al., 1989)). For the present influx ions, charge transfer from

thermal hydrogen in its ground state is the main possibility and this process is strongly selective into particular states of the receiving ion. There is some uncertainty about the targeted levels (Wilson et al., 1988). For the spectral lines of the light impurities exploited in this work, corrections of order 20% may be required, at worst . The spectral consequences of charge transfer however are important, particularly in the vacuum ultraviolet and in lower temperature plasma peripheries than in JET. This will be the subject of a further study.

Acknowledgements:

We are indebted to Drs I Martinson, S Johannsen, U Litzén, M F A Harrison, J Tully and N J Peacock for helpful discussions and pre-publication data. Members of the Applied Mathematics Department at Queen's University, Belfast provided much valuable advice.

REFERENCES

Baluja K L, Burke, P G & Kingston A E (1981) J.Phys.B 14, 119

Behringer K H (1986) Rev. Sci. Instrum. 57, 2000.

Behringer K H, Carolan P G and Denne B et al., (1986) Nucl. Fusion 26, 751.

Behringer K H, Denne, B Forrest M J, Stamp M F, Summers H P, (1985) JET Joint Undertaking report, JET-P(85)31.

Behringer K H, (1987) J. Nucl. Mater. 145-147, 145.

Behringer K H, (1988) J. Nucl. Mater. in print .

Berrington K A, Burke P G, Dufton P L & Kingston A E (1985) At.Data Nucl.Data Tables 33, 195

Blackwell D E, Menon S L R & Petford A D (1984) Mon. Not. R. Astr. Soc. 207, 533

Burgess A (1964) Proc.Symp.Atomic Coll.Processes in Plasmas, Culham, Report AERE-4118

Burgess A & Chidichimo M C (1983) Mon.Not.R.Astr.Soc. 203, 1269

Burgess A & Summers H P (1976) Mon.Not.R.Astr.Soc. 174, 345

Burgess A, Summers H P, Cochrane D M & McWhirter R W P (1977) Mon.Not.R.Astr.Soc. 179, 275

Corliss C & Sugar J (1981) J.Phys.Chem.Ref.Data 10, 200

Corliss C & Sugar J (1982) J.Phys.Chem.Ref.Data 11, 135

Cowan R D (1981) 'The Theory of Atomic Structure & Spectra' (Univ.of California Press)

Eissner W, Jones M A & Nussbaumer H (1974) Comp.Phys.Commun. 8, 270

Fawcett B (1984) At.Data.Nucl.Data Tables 30, 423

Fuhr J R, Martin G A, Weise W L & Younger S M (1981) J.Phys. Chem.Ref.Data 10, 305

Ganas P S (1981) Int.J.Quant.Chem. 20, 1073

Gordon H, Summers H P & Tully J A (1982) Culham Laboratory Report, CLM-R229

Glass R (1979) J.Phys.B. 12, 1633

Henry R J W, Burke P G & Sinfailam A L (1969) Phys.Rev. 178, 218

Ho Y K & Henry R J W (1983) Astrophys.J. 264, 733

Itikawa Y, Hara S, Kato T, Nakazaki S, Pindzola M S & Crandall D H (1983) Nagoya, Institute of Plasma Physics Report IPPJ-AM-27

Johnson L C and Hinnov E, (1973) JQSRT 13, 333.

Kurucz R L & Peytremann E (1975) Smithsonian Astrophysical Observatory, special report 362

Lotz W (1967) Astrophys.J.Supple. 14, 207

Lotz W (1969) F.Phys. 220, 466

McGuire E J (1977) Phys. Rev. A 16, 63

Magee N H, Mann J B, Mertz A L, Robb W D (1977) Los Alamos Scientific Report LA-6691-MS

Man K F, Smith A C H, Harrison M F A (1987) J. Phys. B. - to be published

Mattioli M, Peacock N J, Summers H P, Denne B, Hawkes N C (1989) Phys. Rev. A - submitted

Montague R G, Diserens M J, Harrison M F A (1984) J. Phys. B. 17, 1085

Montague R G, Harrison M F A (1985) J. Phys. B. 18, 1419

Morgan P D et al., (1985) Rev. Sci. Instrum. 56, 862

Nussbaumer H, Pettini M & Storey P J (1981) Astron. & Astrophys. 102, 351

Roth C (1980) At. Data Nucl. Data Tables 25, 118

Smith M W & Weise W L (1971) Astrophys.J.Supple. 23, 103

Stamp M F, Behringer K H, Forrest M J, Morgan P D, Summers H P, (1987) J. Nucl. Mater. 145-147, 236

Stamp M F, Behringer K H, Forrest M J, Morgan P D, Summers H P, (1988) J. Nucl. Mater. in print

Sugar J & Corliss C (1977) J.Phys.Chem.Ref.Data 6, 320

Vainshtein L A, & Sobelman I I (1967) Culham Laboratory Report CLM-Trans 13

Van Regemorter H (1962) Astrophys. J. 136, 906

Weise W L, Smith M W & Glennon B M (1966) U.S Nat.Bureau of Standards, NSRDS-NBS4, vol.1

White H E & Eliason A Y (1933) Phys.Rev. 44, 753

Wilson S M, McCullough R W, Gilbody H B (1988) J. Phys. B. 21, 1027

Younger S M, Fuhr J R, Martin G A & Weise W L (1978) J. Phys. Chem. Ref. Data, 495

TABLE 1a
Ionisation rate coefficient parameters

ion	transition	α_γ	ζ_γ	I_γ/I_H
C^+	$2s^22p\ ^2P \rightarrow 2s^2\ ^1S$	1.00 -0.75	3.0 2.0	1.79209 2.26977
	$2s^22p\ ^2P \rightarrow 2s2p\ ^3P$	0.75	2.0	2.26977
	$2s2p^2\ ^4P \rightarrow 2s^2\ ^1S$	0.00		
	$2s2p^2\ ^4P \rightarrow 2s2p\ ^3P$	1.00	3.0	1.87762
C^{+2}	$2s^2\ ^1S \rightarrow 2s^2S$	1.00	2.0	3.51944
	$2s2p\ ^3P \rightarrow 2s^2S$	1.00	2.0	3.04176
O^{+1}	$2s^22p^3\ ^4S \rightarrow 2s^22p^2\ ^3P$	1.00 -0.625	5.0 2.0	2.58107 3.13080
	$2s^22p^3\ ^4S \rightarrow 2s^22p^2\ ^1D$	0.00		
	$2s^22p^3\ ^4S \rightarrow 2s^22p^2\ ^1S$	0.00		
	$2s^23p^3\ ^4S \rightarrow 2s2p^3\ ^5S$	0.625	2.0	3.13080
	$2s^22p^3\ ^2D \rightarrow 2s^22p^2\ ^3P$	1.00 -0.35714 -0.04286 0.17143	5.0 5.0 5.0 2.0	2.33667 2.52139 2.73019 2.88639
	$2s^22p^3\ ^2D \rightarrow 2s^22p^2\ ^1D$	0.35714 -0.02381 -0.14286	5.0 5.0 3.0	2.52139 2.73019 2.88639
	$2s^22p^3\ ^2D \rightarrow 2s^22p^2\ ^1S$	0.06667 -0.02857	5.0 2.0	2.73019 2.88639
	$2s^22p^3\ ^2D \rightarrow 2s2p^3\ ^5S$	0.00		
	$2s^22p^3\ ^2P \rightarrow 2s^22p^2\ ^3P$	1.00 -0.35714 -0.04286 -0.17143	5.0 5.0 5.0 2.0	2.21230 2.39702 2.60582 2.76202
	$2s^22p^3\ ^2P \rightarrow 2s^22p^2\ ^1D$	0.35714 -0.02381 -0.14286	5.0 5.0 2.0	2.39702 2.60582 2.76202
	$2s^22p^3\ ^2P \rightarrow 2s^22p^2\ ^1S$	0.06667 -0.02857	5.0 2.0	2.60582 2.76202
	$2s^22p^3\ ^2P \rightarrow 2s2p^3$	0.00		
O^{+2}	$2s^22p^2\ ^3P \rightarrow 2s^22p\ ^2P$	1.00 -0.40	4.0 2.0	4.03770 4.69108
	$2s^22p^2\ ^3P \rightarrow 2s2p^2\ ^4P$	0.40	2.0	4.69108
	$2s^22p^2\ ^1D \rightarrow 2s^22p\ ^2P$	1.00	4.0	3.85297
	$2s^22p^2\ ^1D \rightarrow 2s\ 2p^2\ ^4P$	0.00		
	$2s^22p^2\ ^1S \rightarrow 2s^22p\ ^2P$	1.00	4.0	3.64418
	$2s^22p^2\ ^1S \rightarrow 2s2p^2\ ^4P$	0.00		

TABLE 1b

Ionisation rate coefficient parameters (summed over final states)

Ion	Initial State	I_γ/I_H
Cr^{+0}	$3d^5(^6S)4s\ ^7S$	0.49728
	$4s\ ^5S$	0.42809
	$3d^4(^5D)4s^2\ ^5D$	0.42158
	$3d^5(^4G)4s\ ^5G$	0.31029
	$4s\ ^3G$	0.26911
	$3d^6\ ^5D$	0.17471
Cr^{+1}	$3d^5\ ^6S$	1.21253
	$3d^5\ ^4G$	1.02560
	$3d^4(^5D)4s\ ^6D$	1.09865
	$4s\ ^4D$	1.0
	$3d^4(^3H)4s\ ^4H$	0.93558
	$4s\ ^2H$	0.89529
Fe^{+0}	$3d^6(^5D)4s^2\ ^5D$	0.57847
	$3d^7(^4F)4s\ ^5F$	0.51534
	$4s\ ^3F$	0.46934
	$3d^7(^4P)4s\ ^5P$	0.41855
	$3s\ 3p$	0.37036
	$3d^8\ ^3F$	0.27890
Fe^{+1}	$3d^4(^5D)4s\ ^6D$	1.18978
	$4s\ ^4D$	1.11729
	$3d^7\ ^4F$	1.17272
	$3d^7\ ^2G$	1.04539
	$3d^6(^3H)4s\ ^4H$	0.99612
	$4s\ ^2H$	0.95130
	$3d^5(^6S)4s^2\ ^6S$	0.97729
Ni^{+0}	$3d^8(^3F)4s^2\ ^3F$	0.56134
	$3d^9(^2D)4s\ ^3D$	0.55947
	$4s\ ^1D$	0.53027
	$3d^{10}\ ^1S$	0.42712
	$3d^8(^1D)4s^2\ ^1D$	0.43813
Ni^{+1}	$3d^9\ ^2D$	1.33539
	$3d^8(^3F)4s\ ^4F$	1.25890
	$4s\ ^2F$	1.21191
	$3d^8(^3P)4s\ ^4P$	1.12481
	$4s\ ^2P$	1.07047
	$3d^7(^4F)4s^2\ ^4F$	0.87022

TABLE 2

Index of metastable terms and principal spectrum lines for light elements

Ion	Metastable term	Index
C^{+1}	$2s^2 2p\ ^2P$	1
	$2s2p^2\ ^4P$	2
C^{+2}	$2s^2\ ^1S$	1
	$2s2p\ ^3P$	2
O^{+1}	$2s^2 2p^3\ ^4S$	1
	$2s^2 2p^3\ ^2D$	2
	$2s^2 2p^3\ ^2P$	3
O^{+2}	$2s^2 2p^2\ ^3P$	1
	$2s^2 2p^2\ ^1D$	2
	$2s^2 2p^2\ ^1S$	3

Ion	Multiplet	J-J'	Index	λ(Å)air
C^{+1}	$2s^2(^1S)3p\ ^2P - 2s^2(^1S)3s\ ^2S$	3/2-1/2	1	6578.03
	$2s2p(^3P)3p\ ^4P - 2s2p(^3P)3s\ ^4P$	5/2-5/2	2	5145.16
C^{+2}	$2s(^2S)3d\ ^1D - 2s(^2S)3p\ ^1P$	2-1	1	5696.00
	$2s(^2S)3p\ ^3P - 2s(^2S)3s\ ^3S$	2-1	2	4647.40
O^{+1}	$2p^2(^3P)3p\ ^4S - 2p^2(^3P)3s\ ^4P$	3/2-5/2	1	3749.49
	$2p^2(^3P)3p\ ^2P - 2p^2(^3P)3s\ ^2P$	3/2-3/2	2	3973.26
	$2p^2(^3P)3p\ ^2D - 2p^2(^3P)3p\ ^2P$	5/2-3/2	3	4414.91
O^{+2}	$2p(^2P)3p\ ^3D - 2p(^2P)3s\ ^3P$	3-2	1	3759.87
	$2p(^2P)3p\ ^1P - 2p(^2P)3p\ ^1P$	1-1	2	5592.37
	$2p(^2P)3p\ ^1D - 2p(^2P)3s\ ^1P$	2-1	3	2983.78

TABLE 3a

Tabulation of $N_e S_0 W_{0\rho}^{-1}$ for C^{+1}

meta index	line index	T_e(eV)	Electron density (cm^{-3})						
			1.00^{11}	1.00^{12}	1.00^{13}	5.00^{13}	1.00^{14}	1.00^{15}	1.00^{16}
1	1	1.0	2.74^{-4}	2.76^{-4}	2.97^{-4}	3.85^{-4}	4.90^{-4}	1.65^{-3}	4.13^{-3}
	2		–	–	–	–	–	–	–
	1	2.0	3.14^{-2}	3.17^{-2}	3.44^{-2}	4.62^{-2}	6.00^{-2}	2.02^{-1}	4.39^{-1}
	2		–	–	–	–	–	–	–
	1	5.0	9.22^{-1}	9.32^{-1}	1.02	1.42	1.87	6.28	1.25^{1}
	2		–	–	–	–	–	–	–
	1	10.0	4.12	4.16	4.58	6.33	8.32	2.72^{1}	5.08^{1}
	2		–	–	–	–	–	–	–
	1	20.0	1.12^{1}	1.13^{1}	1.23^{1}	1.67^{1}	2.17^{1}	6.76^{1}	1.19^{2}
	2		–	–	–	–	–	–	–
	1	50.0	2.64^{1}	2.66^{1}	2.87^{1}	3.37^{1}	4.71^{1}	1.33^{2}	2.20^{2}
	2		–	–	–	–	–	–	–
	1	100.0	3.79^{1}	3.81^{1}	4.06^{1}	5.10^{1}	6.28^{1}	1.69^{2}	2.75^{2}
	2		–	–	–	–	–	–	–
2	1	1.0	–	–	–	–	–	–	–
	2		4.30^{-4}	4.36^{-4}	5.04^{-4}	7.91^{-4}	1.13^{-3}	4.72^{-3}	1.07^{-2}
	1	2.0	–	–	–	–	–	–	–
	2		4.02^{-2}	4.09^{-2}	4.77^{-2}	7.63^{-2}	1.09^{-1}	4.37^{-1}	8.80^{-1}
	1	5.0	–	–	–	–	–	–	–
	2		9.33^{-1}	9.49^{-1}	1.10	1.76	2.52	9.96	1.97^{1}
	1	10.0	–	–	–	–	–	–	–
	2		3.51	3.57	4.12	6.45	9.14	3.61^{1}	7.20^{1}
	1	20.0	–	–	–	–	–	–	–
	2		8.30	8.42	9.56	1.45^{1}	2.02^{1}	7.90^{1}	1.62^{2}
	1	50.0	–	–	–	–	–	–	–
	2		1.69^{1}	1.71^{1}	1.90^{1}	2.72^{1}	3.68^{1}	1.40^{2}	2.97^{2}
	1	100.0	–	–	–	–	–	–	–
	2		2.37^{1}	2.39^{1}	2.62^{1}	3.58^{1}	4.72^{1}	1.74^{2}	3.78^{2}

TABLE 3b

Tabulation of $N_e S_o W_{o\rho}^{-1}$ for C^{+2}

meta index	line index	T_e(eV)	Electron density (cm^{-3})						
			1.00^{11}	1.00^{12}	1.00^{13}	5.00^{13}	1.00^{14}	1.00^{15}	1.00^{16}
1	1	1.0	3.65^{-5}	3.65^{-5}	3.60^{-5}	3.41^{-5}	3.17^{-5}	1.13^{-5}	2.67^{-6}
	2		–	–	–	–	–	–	–
	1	2.0	6.24^{-2}	6.24^{-2}	6.18^{-2}	5.95^{-2}	5.65^{-2}	2.67^{-2}	7.41^{-3}
	2		–	–	–	–	–	–	–
	1	5.0	7.50	7.50	7.46	7.28	7.06	4.30	1.36
			–	–	–	–	–	–	–
	1	10.0	4.41^{1}	4.41^{1}	4.40^{1}	4.32^{1}	4.23^{1}	2.94^{1}	1.02^{1}
	2		–	–	–	–	–	–	–
	1	20.0	1.20^{2}	1.20^{2}	1.20^{2}	1.18^{2}	1.16^{2}	8.68^{1}	3.38^{1}
	2		–	–	–	–	–	–	–
	1	50.0	2.45^{2}	2.45^{2}	2.45^{2}	2.42^{2}	2.40^{2}	1.95^{2}	8.09^{1}
	2		–	–	–	–	–	–	–
	1	100.0	3.42^{2}	3.42^{2}	3.41^{2}	3.38^{2}	3.35^{2}	2.79^{2}	1.20^{2}
	2		–	–	–	–	–	–	–
2	1	1.0	–	–	–	–	–	–	–
	2		9.02^{-9}	9.13^{-9}	1.02^{-8}	1.50^{-8}	2.08^{-8}	1.11^{-7}	4.59^{-7}
	1	2.0	–	–	–	–	–	–	–
	2		8.29^{-5}	8.39^{-5}	9.43^{-5}	1.40^{-4}	1.96^{-4}	1.03^{-3}	3.75^{-3}
	1	5.0	–	–	–	–	–	–	–
	2		3.09^{-2}	3.13^{-2}	3.48^{-2}	5.02^{-2}	6.91^{-2}	3.51^{-1}	1.30
	1	10.0	–	–	–	–	–	–	–
	2		3.04^{-1}	3.07^{-1}	3.37^{-1}	4.70^{-1}	6.33^{-1}	3.10	1.20^{1}
	1	20.0	–	–	–	–	–	–	–
	2		1.20	1.21	1.31	1.76	2.32	1.08^{1}	4.39^{1}
	1	50.0	–	–	–	–	–	–	–
	2		3.48	3.50	3.73	4.77	6.05	2.61^{1}	1.12^{2}
	1	100.0	–	–	–	–	–	–	–
	2		5.65	5.68	5.99	7.38	9.10	3.64^{1}	1.60^{2}

TABLE 3c

Tabulation of $N_e S_\sigma W_{\sigma\rho}^{-1}$ for O^{+1}

meta index	line index	T_e(eV)	Electron density (cm^{-3})						
			1.00^{11}	1.00^{12}	1.00^{13}	5.00^{13}	1.00^{14}	1.00^{15}	1.00^{16}
1	1	1.0	2.60^{-4}	2.61^{-4}	2.67^{-4}	2.93^{-4}	3.25^{-4}	8.07^{-4}	2.45^{-3}
	2		–	–	–	–	–	–	–
	3		–	–	–	–	–	–	–
	1	2.0	4.17^{-2}	4.18^{-2}	4.27^{-2}	4.69^{-2}	5.20^{-2}	1.26^{-1}	3.49^{-1}
	2		–	–	–	–	–	–	–
	3		–	–	–	–	–	–	–
	1	5.0	1.35	1.35	1.39	1.53	1.71	4.21	1.12^{1}
	2		–	–	–	–	–	–	–
	3		–	–	–	–	–	–	–
	1	10.0	5.87	5.88	6.03	6.65	7.42	1.83^{1}	4.39^{1}
	2		–	–	–	–	–	–	–
	3		–	–	–	–	–	–	–
	1	20.0	1.53^{1}	1.54^{1}	1.57^{1}	1.72^{1}	1.91^{1}	4.60^{1}	1.26^{2}
	2		–	–	–	–	–	–	–
	3		–	–	–	–	–	–	–
	1	50.0	3.47^{1}	3.48^{1}	3.55^{1}	3.84^{1}	4.21^{1}	9.52^{1}	2.63^{2}
	2		–	–	–	–	–	–	–
	3		–	–	–	–	–	–	–
	1	100.0	5.30^{1}	5.31^{1}	5.40^{1}	5.80^{1}	6.28^{1}	1.34^{2}	3.62^{2}
	2		–	–	–	–	–	–	–
	3		–	–	–	–	–	–	–
2	1	1.0	–	–	–	–	–	–	–
	2		-4.57^{-5}	-4.60^{-5}	-4.88^{-5}	-6.18^{-5}	-7.93^{-5}	-5.38^{-4}	-7.96^{-3}
	3		1.56^{-4}	1.57^{-4}	1.66^{-4}	2.08^{-4}	2.58^{-4}	1.04^{-3}	6.33^{-3}
	1	2.0	–	–	–	–	–	–	–
	2		-6.45^{-3}	-6.49^{-3}	-6.91^{-3}	-8.84^{-3}	-1.14^{-2}	-7.29^{-2}	-8.82^{-1}
	3		2.55^{-2}	2.57^{-2}	2.73^{-2}	3.42^{-2}	4.27^{-2}	1.67^{-1}	8.52^{-1}
	1	5.0	–	–	–	–	–	–	–
	2		-1.96^{-1}	-1.98^{-1}	-2.12^{-1}	-2.77^{-1}	-3.61^{-1}	-2.22	-2.14^{1} (U)
	3		8.36^{-1}	8.42^{-1}	8.99^{-1}	1.15	1.45	5.68	2.46^{1} (A)
	1	10.0	–	–	–	–	–	–	–
	2		-8.28^{-1}	-8.34^{-1}	-8.94^{-1}	-1.17	-1.52	-9.02	-7.40^{1}
	3		3.58	3.60	3.85	4.91	6.20	2.43^{1}	9.55^{1}
	1	20.0	–	–	–	–	–	–	–
	2		-2.14	-2.16	-2.30	-2.97	-3.82	-2.15^{1}	-1.77^{2}
	3		9.24	9.30	9.89	1.25^{1}	1.56^{1}	5.96^{1}	2.37^{2}
	1	50.0	–	–	–	–	–	–	–
	2		-4.88	-4.91	-5.20	-6.50	-8.17	-4.18^{1}	-3.22^{2}
	3		2.07^{1}	2.08^{1}	2.20^{1}	2.69^{1}	3.29^{1}	1.19^{2}	4.60^{2}
	1	100.0	–	–	–	–	–	–	–
	2		-7.47	-7.51	-7.89	-9.64	-1.19^{1}	-5.60^{1}	-4.07^{2}
	3		3.10^{1}	3.11^{1}	3.26^{1}	3.91^{1}	4.70^{1}	1.60^{2}	6.04^{2}
3	1	1.0	–	–	–	–	–	–	–
	2		3.00^{-4}	3.01^{-4}	3.16^{-4}	3.80^{-4}	4.59^{-4}	1.68^{-3}	1.02^{-2}
	3		-1.27^{-5}	-1.28^{-5}	-1.38^{-5}	-1.86^{-5}	-2.52^{-5}	-2.23^{-4}	-3.72^{-3}
	1	2.0	–	–	–	–	–	–	–
	2		4.19^{-2}	4.21^{-2}	4.42^{-2}	5.35^{-2}	6.49^{-2}	2.31^{-1}	1.22
	3		-2.10^{-3}	-2.12^{-3}	-2.30^{-3}	-3.15^{-3}	-4.31^{-3}	-3.70^{-2}	-5.28^{-1}
	1	5.0	–	–	–	–	–	–	–
	2		1.24	1.25	1.32	1.62	1.98	7.10	3.20^{1}
	3		-7.08^{-2}	-7.15^{-2}	-7.83^{-2}	-1.10^{-1}	-1.52^{-1}	-1.24	-1.46^{1}
	1	10.0	–	–	–	–	–	–	–
	2		5.14	5.17	5.46	6.70	8.21	2.92^{1}	1.23^{2}
	3		-3.08^{-1}	-3.11^{-1}	-3.41^{-1}	-4.78^{-1}	-6.59^{-1}	-5.11	-5.54^{1}
	1	20.0	–	–	–	–	–	–	–
	2		1.29^{1}	1.30^{1}	1.37^{1}	1.66^{1}	2.02^{1}	6.99^{1}	2.82^{2}
	3		-8.05^{-1}	-8.12^{-1}	-8.85^{-1}	-1.22	-1.66	-1.20^{1}	-1.24^{2}
	1	50.0	–	–	–	–	–	–	–
	2		2.85^{1}	2.86^{1}	2.99^{1}	3.54^{1}	4.22^{1}	1.38^{2}	5.27^{2}
	3		-1.87	-1.88	-2.03	-2.68	-3.54	-2.29^{1}	-2.21^{2}
	1	100.0	–	–	–	–	–	–	–
	2		4.21^{1}	4.23^{1}	4.39^{1}	5.11^{1}	5.98^{1}	1.83^{2}	6.74^{2}
	3		-2.87	-2.89	-3.09	-3.97	-5.11	-3.02^{1}	-2.73^{2}

TABLE 3d

Tabulation of $N_e S_o W_{op}^{-1}$ for O^{+2}

meta index	line index	T_e(eV)	Electron density (cm^{-3})						
			1.00^{11}	1.00^{12}	1.00^{13}	5.00^{13}	1.00^{14}	1.00^{15}	1.00^{16}
1	1	1.0	2.11^{-6}	2.11^{-6}	2.18^{-6}	2.46^{-6}	2.81^{-6}	7.56^{-6}	1.91^{-7}
	2		–	–	–	–	–	–	–
	3		–	–	–	–	–	–	–
	1	2.0	4.1^{-4}	4.11^{-4}	4.20^{-4}	4.60^{-4}	5.08^{-4}	1.17^{-3}	2.79^{-3}
	2		–	–	–	–	–	–	–
	3		–	–	–	–	–	–	–
	1	5.0	2.23^{-1}	2.23^{-1}	2.27^{-1}	2.42^{-1}	2.60^{-1}	5.17^{-1}	1.25
	2		–	–	–	–	–	–	–
	3		–	–	–	–	–	–	–
	1	10.0	2.44	2.44	2.47	2.60	2.76	5.11	1.31^{1}
	2		–	–	–	–	–	–	–
	3		–	–	–	–	–	–	–
	1	20.0	1.04^{1}	1.04^{1}	1.05^{1}	1.09^{1}	1.15^{1}	2.00^{1}	5.26^{1}
	2		–	–	–	–	–	–	–
	3		–	–	–	–	–	–	–
	1	50.0	3.30^{1}	3.30^{1}	3.33^{1}	3.44^{1}	3.58^{1}	5.77^{1}	1.51^{2}
	2		–	–	–	–	–	–	–
	3		–	–	–	–	–	–	–
	1	100.0	5.78^{1}	5.78^{1}	5.82^{1}	5.98^{1}	6.19^{1}	9.39^{1}	2.38^{2}
	2		–	–	–	–	–	–	–
	3		–	–	–	–	–	–	–
2	1	1.0	–	–	–	–	–	–	–
	2		-5.56^{-9}	-5.61^{-9}	-6.04^{-9}	-7.99^{-9}	-1.04^{-8}	-5.59^{-8}	-5.24^{-7}
	3		2.54^{-8}	2.54^{-8}	2.58^{-8}	2.73^{-8}	2.92^{-8}	6.38^{-8}	3.83^{-7}
	1	2.0	–	–	–	–	–	–	–
	2		-1.34^{-4}	-1.35^{-4}	-1.44^{-4}	-1.84^{-4}	-2.33^{-4}	-1.13^{-3}	-9.40^{-3}
	3		2.37^{-4}	2.37^{-4}	2.41^{-4}	2.54^{-4}	2.71^{-4}	5.72^{-4}	3.07^{-3}
	1	5.0	–	–	–	–	–	–	–
	2		-8.31^{-2}	-8.36^{-2}	-8.88^{-2}	-1.12^{-1}	-1.41^{-1}	-6.45^{-1}	-4.55
	3		8.84^{-2}	8.85^{-2}	8.97^{-2}	9.47^{-2}	1.01^{-1}	2.10^{-1}	1.01
	1	10.0	–	–	–	–	–	–	–
	2		-8.92^{-1}	-8.98^{-1}	-9.51^{-1}	-1.19	-1.48	-6.61	-4.45^{1}
	3		8.62^{-1}	8.63^{-1}	8.73^{-1}	9.18^{-1}	9.75^{-1}	1.96	9.07
	1	20.0	–	–	–	–	–	–	–
	2		-3.51	-3.53	-3.72	-4.57	-5.64	-2.43^{1}	-1.63^{2}
	3		3.41	3.41	3.45	3.61	3.81	7.31	3.26^{1}
	1	50.0	–	–	–	–	–	–	–
	2		-8.93	-8.97	-9.39	-1.13^{1}	-1.36^{1}	-5.55^{1}	-3.90^{2}
	3		9.79	9.80	9.89	1.03^{1}	1.08^{1}	1.92^{1}	8.10^{1}
	1	100.0	–	–	–	–	–	–	–
	2		-1.31^{1}	-1.32^{1}	-1.37^{1}	-1.61^{1}	-1.91^{1}	-7.34^{1}	-5.40^{2}
	3		1.67^{1}	1.67^{1}	1.69^{1}	1.74^{1}	1.81^{1}	3.03^{1}	1.21^{2}
3	1	1.0	–	–	–	–	–	–	–
	2		2.99^{-6}	3.01^{-6}	3.23^{-6}	4.23^{-6}	5.44^{-6}	2.33^{-7}	9.83^{-7}
	3		-3.61^{-8}	-3.61^{-8}	-3.66^{-8}	-3.86^{-8}	-4.11^{-8}	-8.18^{-8}	-3.76^{-7}
	1	2.0	–	–	–	–	–	–	–
	2		7.21^{-4}	7.25^{-4}	7.71^{-4}	9.73^{-4}	1.22^{-3}	4.89^{-3}	2.03^{-2}
	3		-3.33^{-4}	-3.34^{-4}	-3.38^{-4}	-3.55^{-4}	-3.77^{-4}	-7.47^{-4}	-3.32^{-3}
	1	5.0	–	–	–	–	–	–	–
	2		4.46^{-1}	4.49^{-1}	4.76^{-1}	5.94^{-1}	7.39^{-1}	2.88	1.13
	3		-1.18^{-1}	-1.18^{-1}	-1.19^{-1}	-1.26^{-1}	-1.33^{-1}	-2.63^{-1}	-1.11
	1	10.0	–	–	–	–	–	–	–
	2		4.78	4.81	5.09	6.30	7.78	2.99^{1}	1.18^{2}
	3		-1.07	-1.07	-1.08	-1.13	-1.20	-2.31	-9.45
	1	20.0	–	–	–	–	–	–	–
	2		1.88^{1}	1.89^{1}	1.99^{1}	2.42^{1}	2.96^{1}	1.11^{2}	4.54^{2}
	3		-3.94	-3.94	-3.98	-4.16	-4.38	-8.10	-3.24^{1}
	1	50.0	–	–	–	–	–	–	–
	2		4.88^{1}	4.90^{1}	5.12^{1}	6.09^{1}	7.29^{1}	2.60^{2}	1.13^{3}
	3		-1.01^{1}	-1.02^{1}	-1.02^{1}	-1.06^{1}	-1.11^{1}	-1.93^{1}	-7.54^{1}
	1	100.0	–	–	–	–	–	–	–
	2		7.06^{1}	7.08^{1}	7.36^{1}	8.57^{1}	1.01^{2}	3.41^{2}	1.56^{3}
	3		-1.59^{1}	-1.59^{1}	-1.60^{1}	-1.65^{1}	-1.72^{1}	-2.83^{1}	-1.06^{2}

TABLE 4a

Ion	Metastable Term	Index
Cr^{+0}	$3d^5(^6S)4s\ ^7S$	1
	$3d^5(^6S)4s\ ^5S$	2
	$3d^4(^5D)4s^2\ ^5D$	3
	$3d^5(^4G)4s\ ^5G$	4
	$3d^5(^4G)4s\ ^3G$	5

Ion	Metastable Term	Index
Cr^{+1}	$3d^5\ ^6S$	1
	$3d^5\ ^4G$	2
	$3d^4\ (^5D)4s\ ^6D$	3
	$3d^4(^5D)4s\ ^4D$	4
	$3d^4(^3H)4s\ ^4H$	5
	$3d^4(^3H)4s\ ^2H$	6

Ion	Metastable Term	Index
Fe^{+0}	$3d^6(^5D)4s^2\ ^5D$	1
	$3d^7(^4F)4s\ ^5F$	2
	$3d^7(^4F)4s\ ^3F$	3
	$3d^7(^4P)4s\ ^5P$	4
	$3d^7(^4P)4s\ ^3P$	5

Ion	Metastable term	Index
Fe^{+1}	$3d^6(^5D)4s\ ^6D$	1
	$3d^6(^5D)4s\ ^4D$	2
	$3d^7\ ^4F$	3
	$3d^7\ ^2G$	4
	$3d^6(^3H)4s\ ^4H$	5
	$3d^6(^3H)4s\ ^2H$	6
	$3d^5(^6S)4s^2\ ^6S$	7

Ni^{+0}	$3d^8(^3F)4s^2\ ^3F$	1
	$3d^9(^2D)4s\ ^3D$	2
	$3d^9(^2D)4s\ ^1D$	3
	$3d^{10}\ ^1S$	4

Ni^{+1}	$3d^9\ ^2D$	1
	$3d^8(^3F)4s\ ^4F$	2
	$3d^8(^3F)4s\ ^2F$	3
	$3d^8(^3P)4s\ ^4P$	4
	$3d^8(^3P)4s\ ^2P$	5
	$3d^7(^4F)4s^2\ ^4F$	6

TABLE 4b

Ion	Multiplet Index	Transition Multiplet	Component	λ(A)	Branching Ratio	Metastable Dependence	A-value
Cr^{+0}	1	$3d^5(^6S)4s\ ^7S - 3d^5(^6S)4p\ ^7P$	3-4	4254.35	1.0	1	3.15[7]
	8	$3d^5(^6S)4s\ ^5S - 3d^5(^6S)4p\ ^5P$	2-3	5208.44	0.86	2	5.1[7]
	22	$3d^4(^5D)4s\ ^5D - 3d^4(^5D)4s4p(^1P)\ ^5F$	4-5	3021.56	0.98	3	3.2[8]
	44	$3d^5(^4G)4s\ ^5G - 3d^5(^4G)4p\ ^5H$	6-7	3963.68	1.0	4	1.3[8]
	72	$3d^5(^4G)4s\ ^3G - 3d^5(^4G)4p\ ^3H$	5-6	4922.27	0.89	5	4.0[7]
Cr^{+1}	α	$3d^5\ ^6S - 3d^4(^5D)4p\ ^6P$	5/2-7/2	2055.59	0.40	1	1.97[8]
						3	2.93[8]
	β	$3d^5\ ^4G - 3d^4(^3H)4p\ ^4G$	11/2-11/2	2133.50	0.46	2	1.94[8]
						5	2.05[8]
	1	$3d^4(^5D)4s\ ^6D - 3d^4(^5D)4p\ ^6F$	9/2-11/2	2835.62	1.0	3	2.76[8]
	7	$3d^4(^5D)4s\ ^4D - 3d^4(^5D)4p\ ^4F$	7/2-9/2	3132.03	0.83	4	1.92[8]
	14	$3d^4(^3H)4s\ ^4H - 3d^4(^3H)4p\ ^4I$	13/2-15/2	2822.37	1.0	5	2.70[8]
	25	$3d^4(^3H)4s\ ^2H - 3d^4(^3H)4p\ ^2I$	11/2-13/2	3050.12	0.78	6	1.8[8]
Fe^{+0}	16	$3d^6(^5D)4s^2\ ^5D - 3d^6(^5D)4s4p(^1P)\ ^5F$	4-5	2483.27	0.94	1	4.9[8]
	41	$3d^7(^4F)4s\ ^5F - 3d^7(^4F)4p\ ^5G$	5-6	3581.19	1.0	2	1.02[8]
	59	$3d^7(^4F)4s\ ^3F - 3d^7(^4F)4p\ ^3G$	4-5	4271.76	0.26	3	2.5[7]
						2	7.1[7]
	87	$3d^7(^4P)4s\ ^5P - 3d^7(^4P)4p\ ^5D$	3-4	3407.46	0.70	4	6.0[7]
	216	$3d^7(^4P)4s\ ^3P - 3d^7(^4P)4p\ ^3D$	2-3	4181.75	0.28	5	3.5[7]

TABLE 4b (continued)

Ion	Multiplet Index	Transition Multiplet	Component	λ(A)	Branching Ratio	Metastable Dependence	A-value
Fe^{+1}	α	$3d^6(^5D)4s\ ^6D - 3d^6(^5D)4p\ ^6F$	9/2-11/2	2382.04	1.0	1	3.90^8
	β	$3d^6(^5D)4s\ ^4D - 3d^6(^5D)4p\ ^4F$	7/2-9/2	2755.74	0.88	2	2.52^8
	γ	$3d^7\ ^4F - 3d^6(^3H)\ 4p\ ^4G$	9/2-11/2	1702.04	0.36	3	1.13^8
						5	2.03^8
	δ	$3d^7\ ^2G - 3d^6(^3H)4p\ ^2G$	9/2-9/2	2162.02	0.19	4	3.57^7
						6	1.41^8
	ε	$3d^6(^3H)4s\ ^4H - 3d^6(^3H)4p\ ^4I$	13/2-15/2	2493.26	1.0	5	3.51^8
	32	$3d^6(^3H)4s\ ^2H - 3d^6(^3H)4p\ ^2I$	11/2-13/2	2767.50	0.83	6	2.05^8
	ν	$3d^5(^6S)4s^2\ ^6S - 3d^5(^6S)4s4p(^1P)\ ^6P$	5/2-7/2	1785.27	1.0	7	1.11^9
Ni^{+0}	22	$3d^8(^3F)4s^2\ ^3F - 3d^8(^3F)4s4p(^1P)\ ^3G$	4-5	2320.03	1.0	1	6.93^8
	38	$3d^9(^2D)4s\ ^3D - 3d^9(^2D)4p\ ^3F$	3-4	3414.76	0.90	2	5.5^7
	70	$3d^9(^2D)4s\ ^1D - 3d^9(^2D)4p\ ^1F$	2-3	3619.39	0.82	3	7.3^7
	α	$3d^{10}\ ^1S - 3d^9(^2D)4p\ ^1P$	0-1	5476.90	0.15	4	2.3^7
						3	1.2^8
Ni^{+1}	α	$3d^9\ ^2D - 3d^8(^3F)4p\ ^2D$	5/2-5/2	1741.55	0.21	1	2.0^8
						3	5.0^8
	2	$3d^8(^3F)4s\ ^4F - 3d^8(^3F)4p\ ^4G$	9/2-11/2	2216.48	1.0	2	5.5^8
	10	$3d^8(^3F)4s\ ^2F - 3d^8(^3F)4p\ ^2G$	7/2-9/2	2394.52	0.64	3	2.9^8
						2	1.5^8
	β	$3d^8(^3P)4s\ ^4P - 3d^8(^3P)4p\ ^4D$	5/2-7/2	2097.09	1.0	4	1.2^8
	γ	$3d^8(^3P)4s\ ^2P - 3d^8(^3P)4p\ ^2D$	3/2-5/2	2341.21	0.82	5	3.51^8
						6	1.74^9
	δ	$3d^7(^4F)4s^2\ ^4F - 3d^7(^4F)4s4p(^1P)\ ^4G$	9/2-11/2	1629.28	1.0		

TABLE 5

Influx results for C II and C III ions.

Line (A)	metastable term	S/XB	flux(%)	total flux(%)
C II limiter				
6578 5145	$2s^2 2p\ ^2P$ $2s\ 2p^2\ ^4P$	38 24	7.5 1.4	8.9
C III limiter				
5696 4647	$2s^2\ ^1S$ $2s\ 2p\ ^3P$	342 6.7	2.4 3.5	5.9
C II inner wall				
904 1010	$2s^2\ 2p\ ^2P$ $2s\ 2p^2\ ^4P$	0.80 1.4	5.9 1.0	6.9
C III inner wall				
977 460	$2s^2\ ^1S$ $2s\ 2P\ ^1P$	0.11 0.72	5.3 2.1	7.4

TABLE 6

Influx results for O II and O III ions

Line (A)	metastable term	S/XB	flux(%)	total flux(%)
O II limiter				
3749	$2s^2 2p^3\ {}^4S$	53	0.74	
3973	$2s^2 2p^3\ {}^2P$	42	0.31	1.72
4415	$2s^2 2p^3\ {}^2D$	31	0.67	
O III limiter				
3760	$2s^2 2p^2\ {}^3P$	58	0.84	
3703	$2s^2 2p^2\ {}^5S$	(59)	0.34	
2984	$2s^2 2p^3\ {}^1S$	17	0.3	1.88
5592	$2s^2 2p^3\ {}^1D$	71	0.4	
O III inner wall				
703	$2s^2 2p^2\ {}^3P$	1.2	1.4	≈3(scaled)

TABLE 7

Influx results for Cr I ions

Line (A)	metastable term	S/XB	flux (%)
4254	$3d^5\ 4s\ {}^7S$	3	0.3
5208	$3d^5\ 4s\ {}^5S$	0.9	0.01

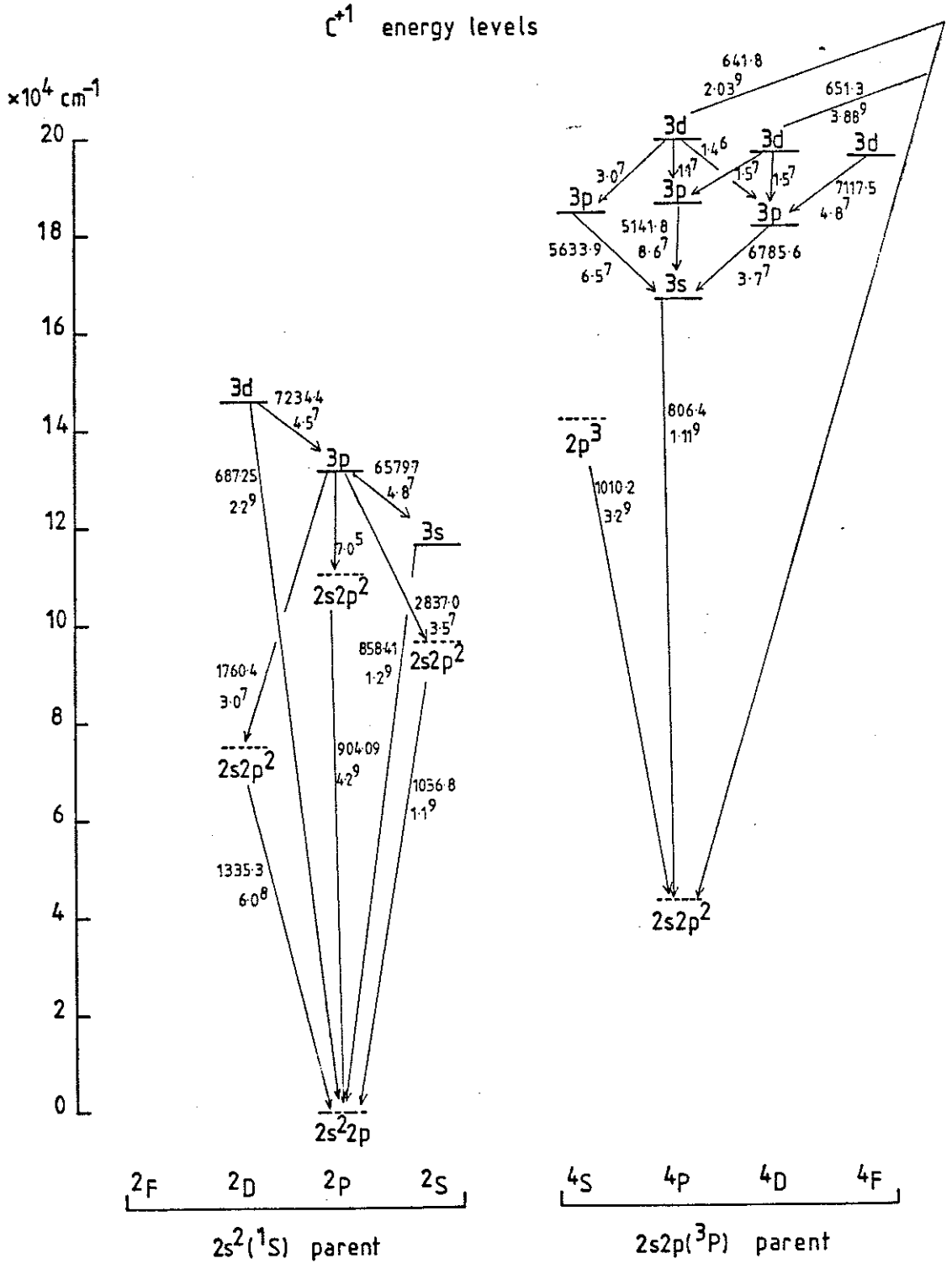

Fig. 1 Energy levels and principal radiative transitions of C^{+1}. (Number pairs are the wavelength (Å) and transition probability (sec^{-1}).

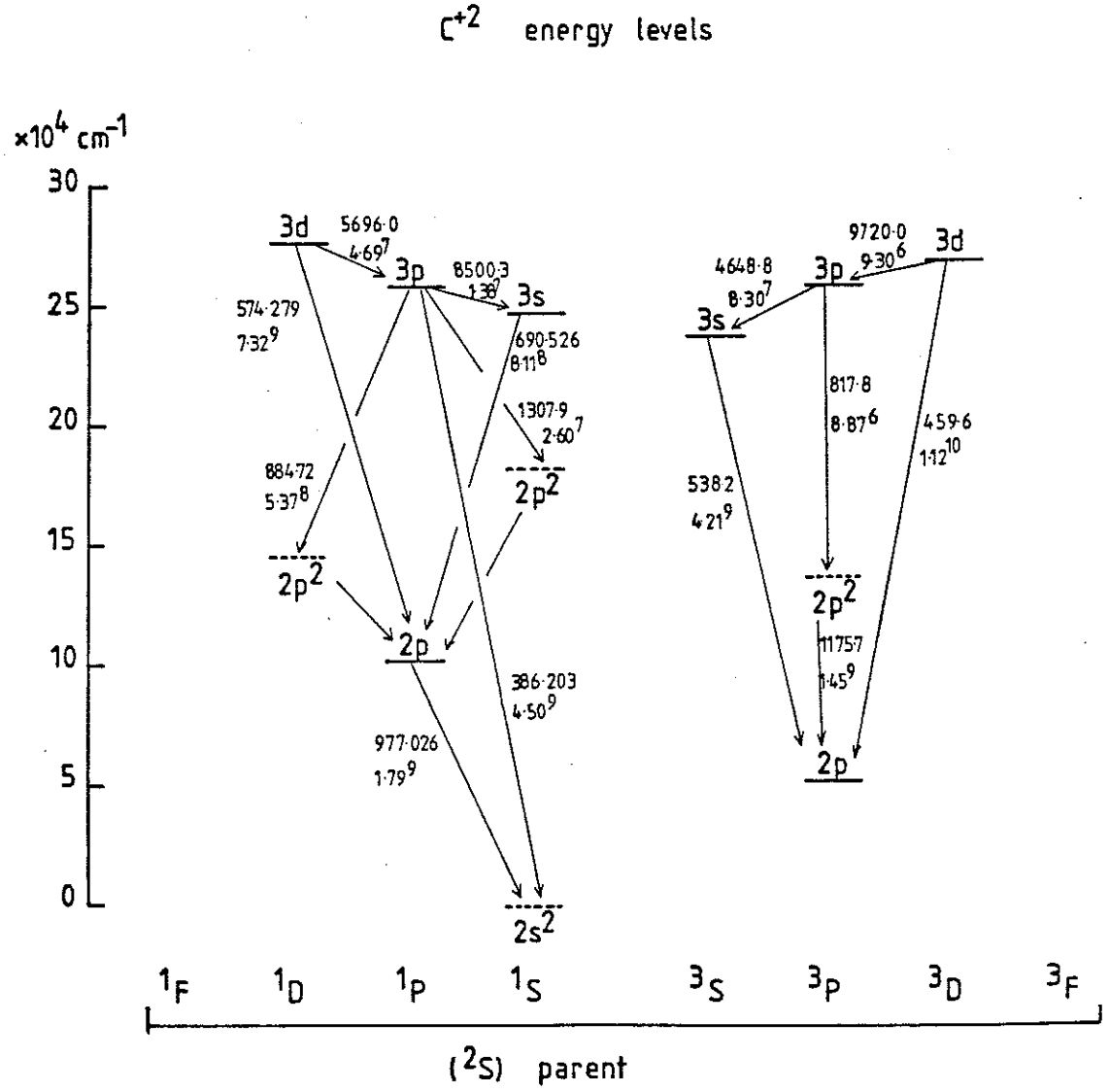

Fig. 2 Energy levels and principal radiative transitions of C^{+2}.

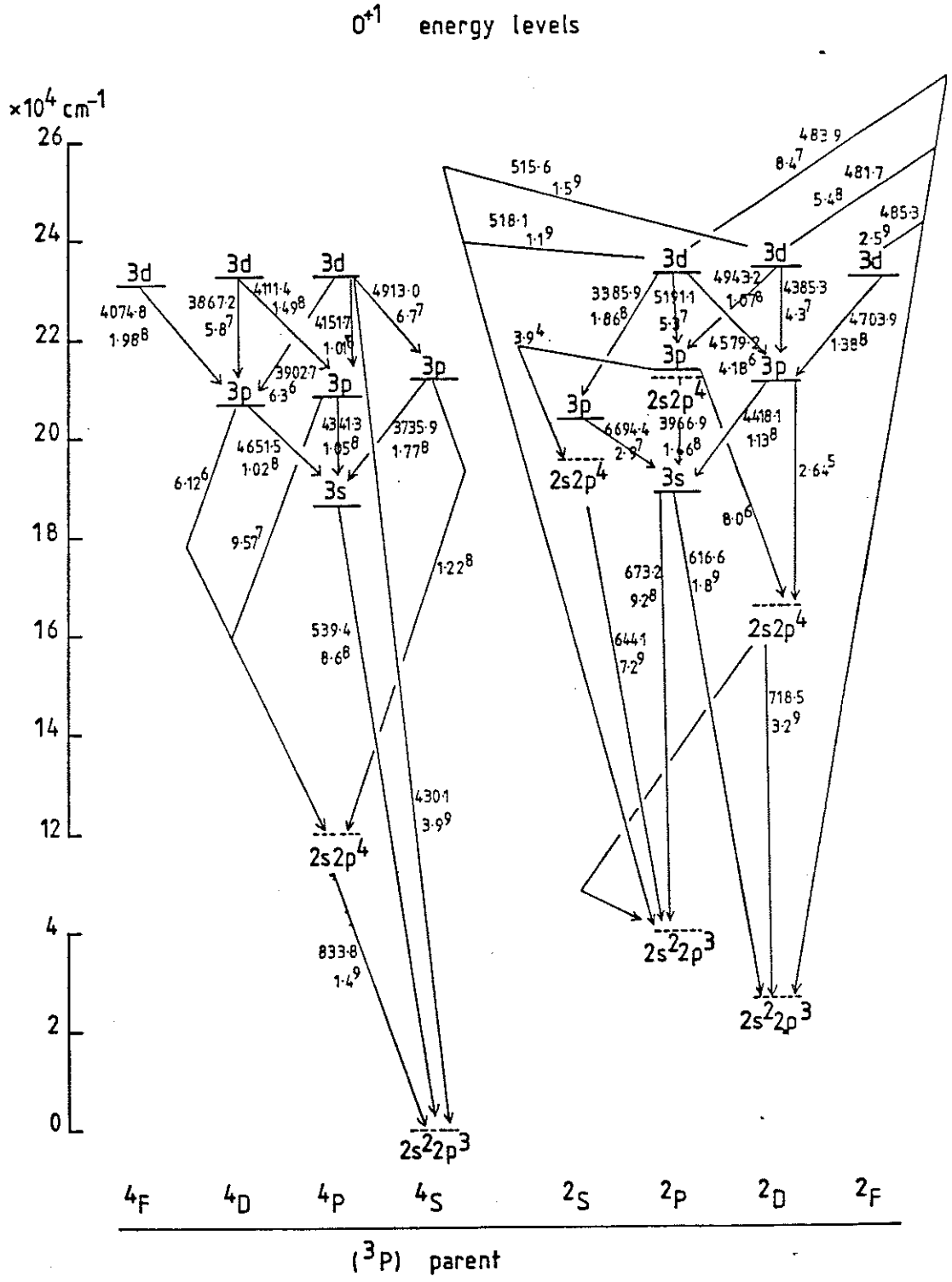

Fig. 3 Energy levels and principal radiative transitions of 0^{+1}.

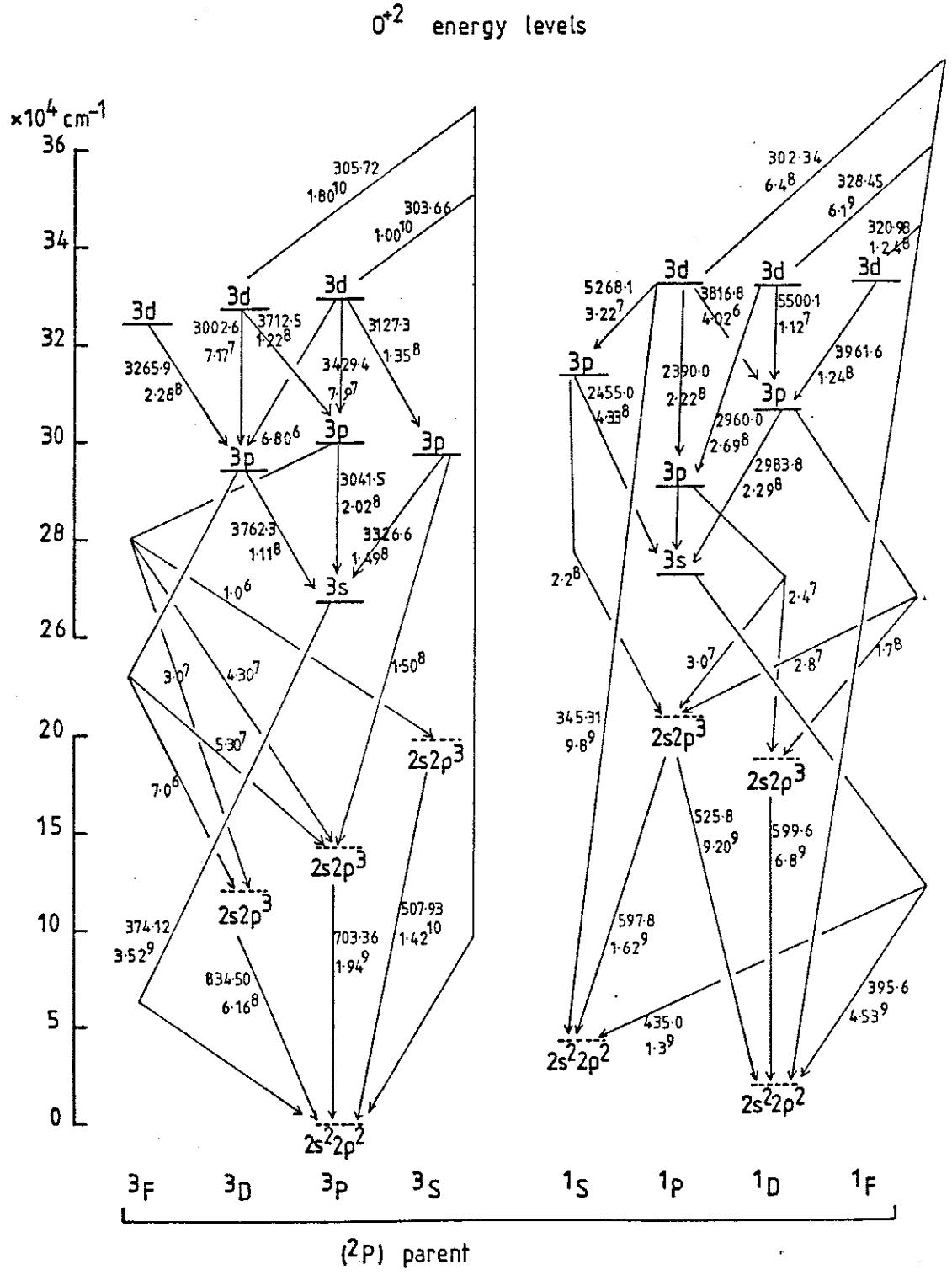

Fig. 4 Energy levels and principal radiative transitions of 0^{+2}.

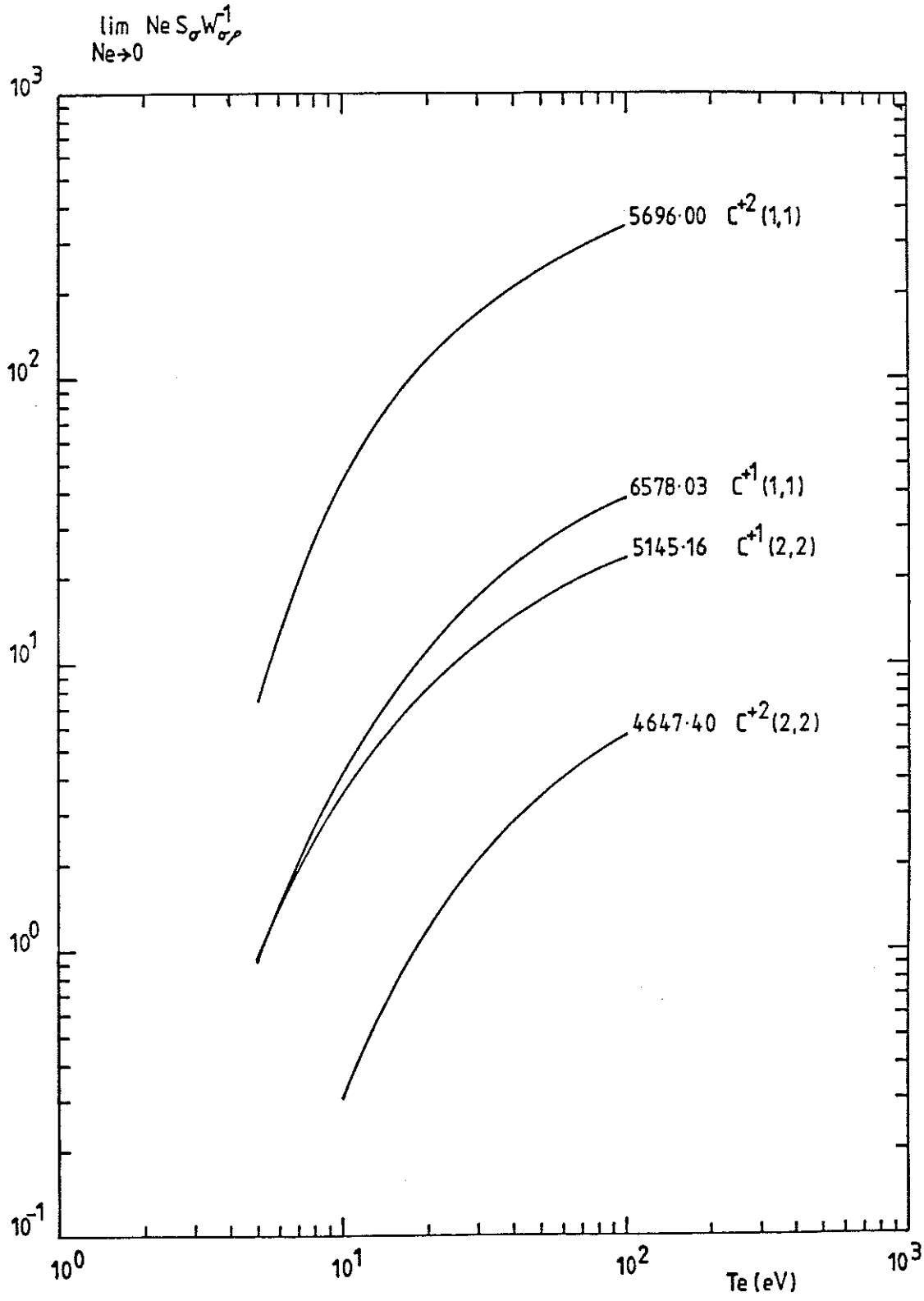

Fig. 5a Ionisations/photon at zero density for C^{+1} and C^{+1}. (Curves are labelled by wavelength and ion. (m,ℓ) denotes metastable m and line ℓ, see Table 2).

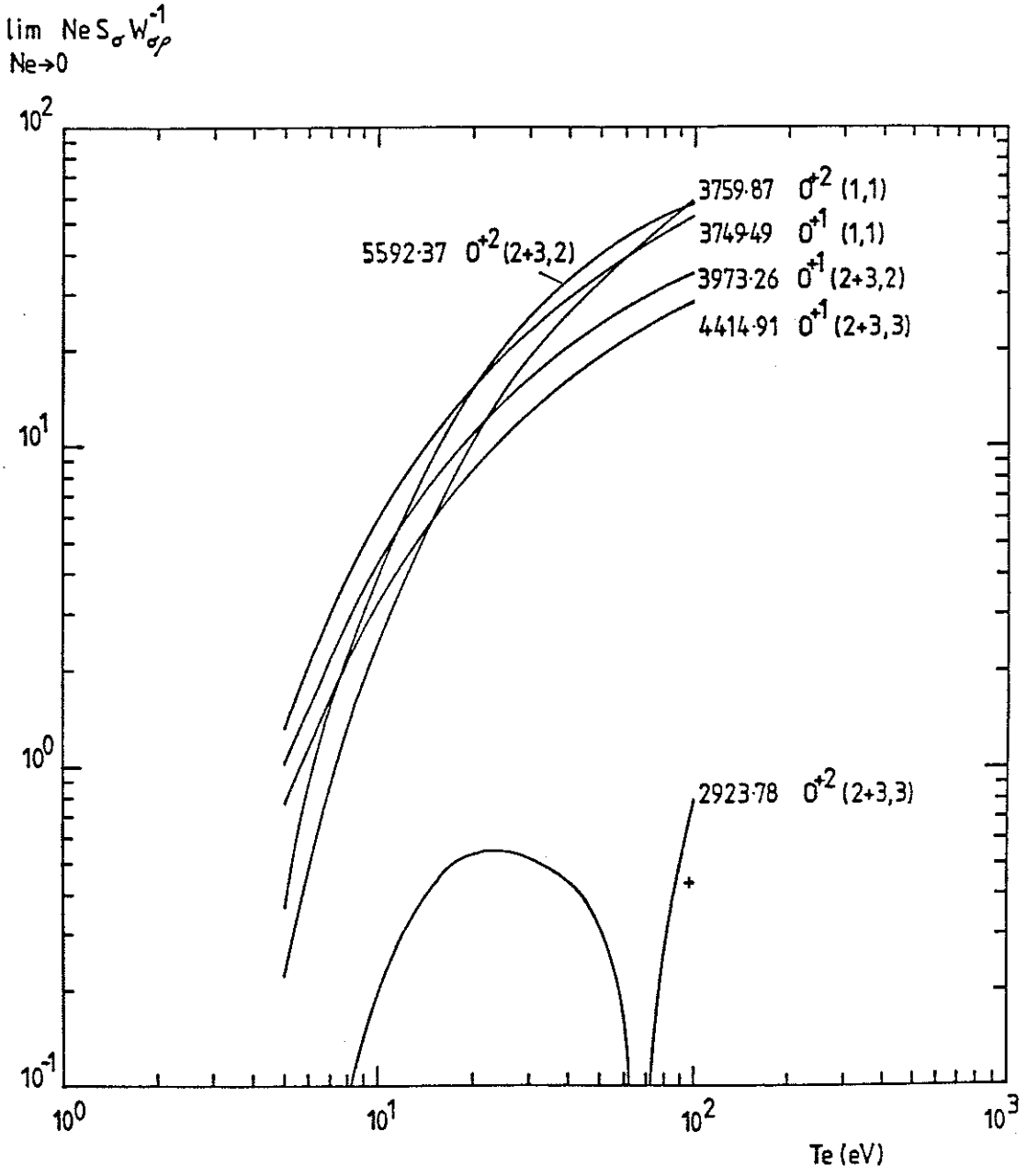

Fig. 5b Ionisations/photon at zero density for 0^{+1} and 0^{+2}.

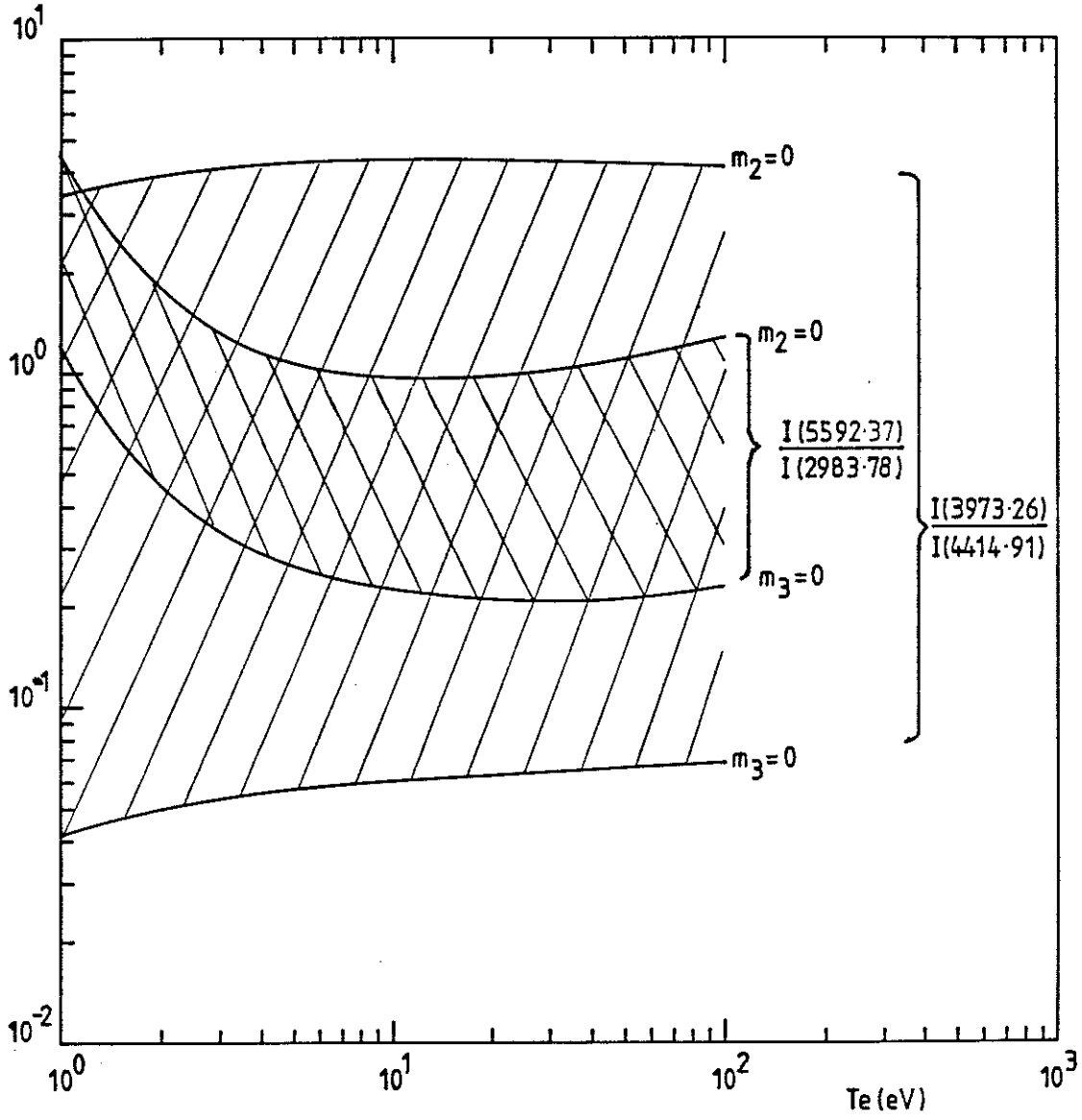

Fig. 5c Limiting intensity ratios for spectrum lines of 0^{+1} and 0^{+1}. ($M\rho=0$, denotes limit with zero fractional abundance for metastable ρ).

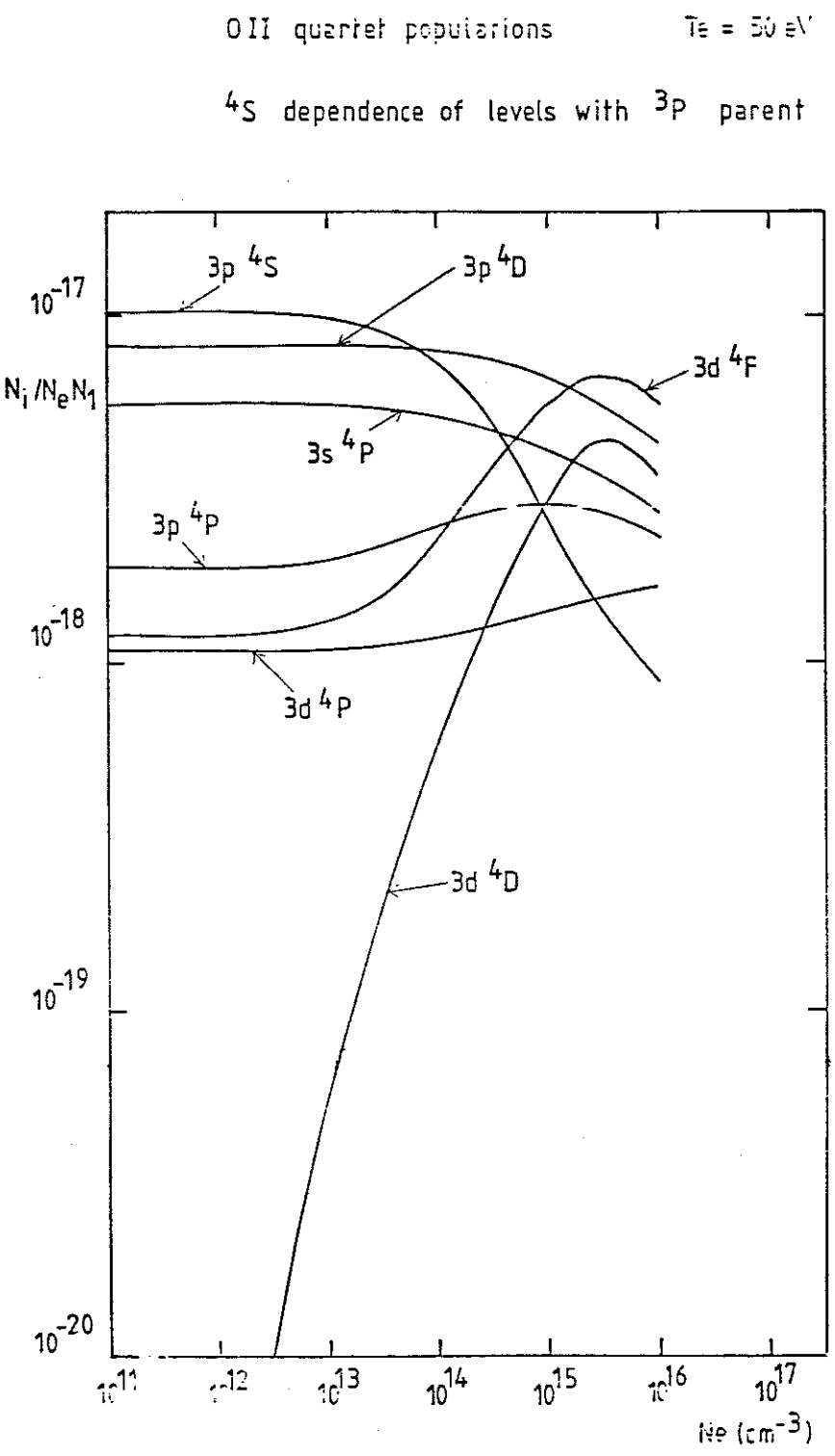

Fig. 6 Excited level populations for 0^{+1}. Dependence on the ^4S ground state of levels with ^3P parent is shown. $T_e = 50\,\text{eV}$.

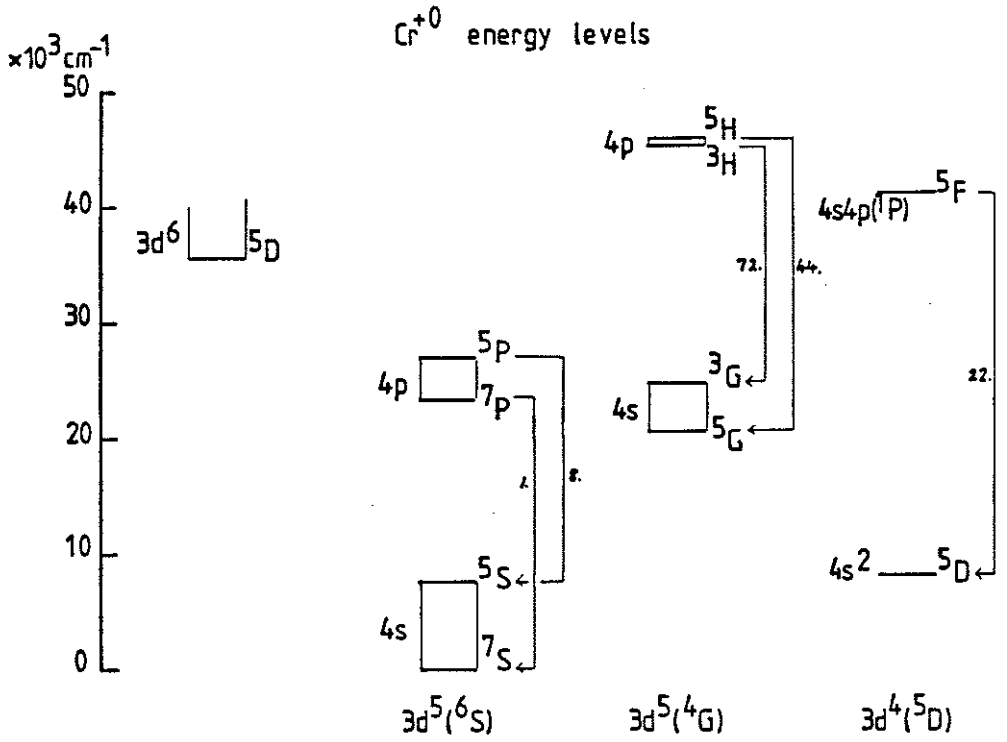

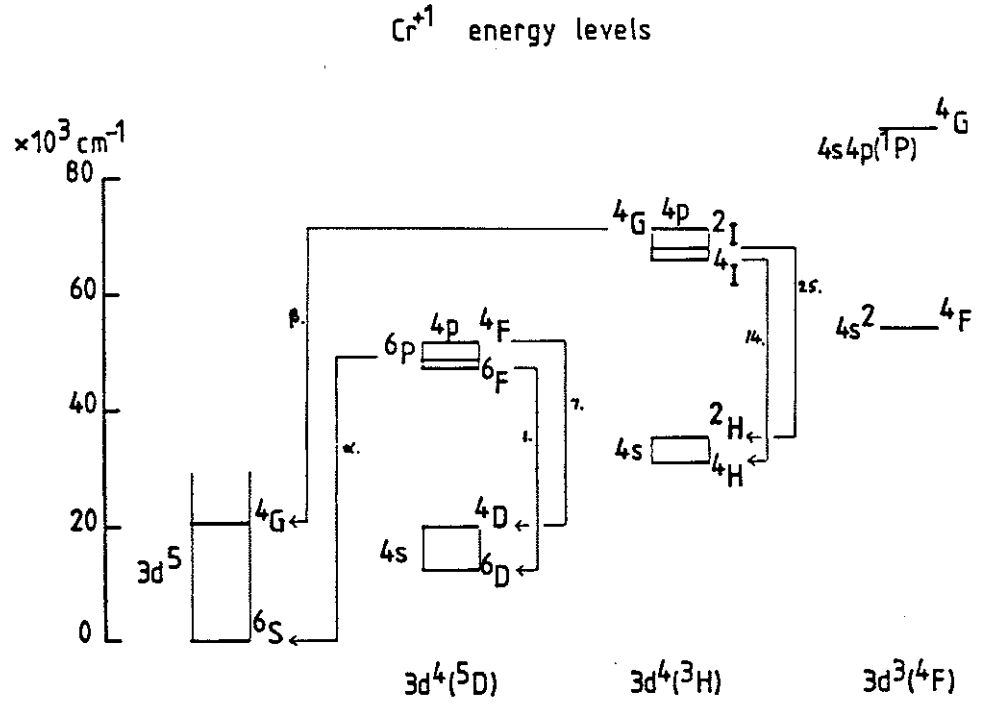

Fig. 7a & 7b Energy levels and principal radiative transitions of Cr^{+0} and Cr^{+1}.

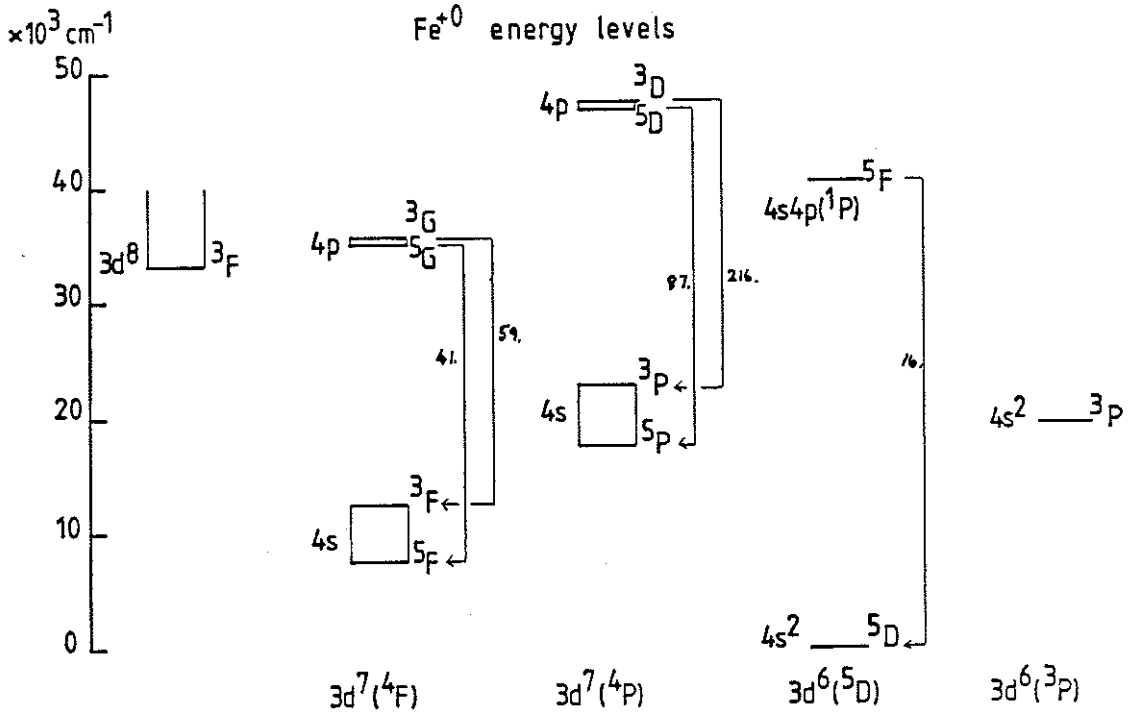

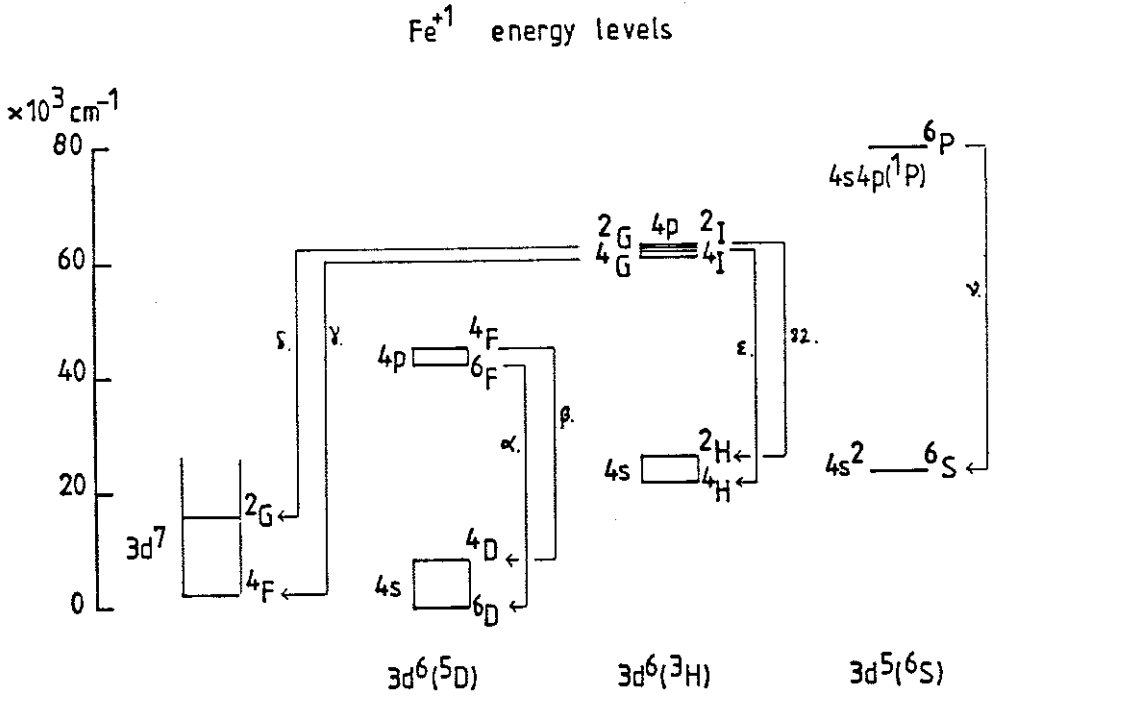

Fig. 8a & 8b Energy levels and principal radiative transitions of Fe^{+0} and Fe^{+1}.

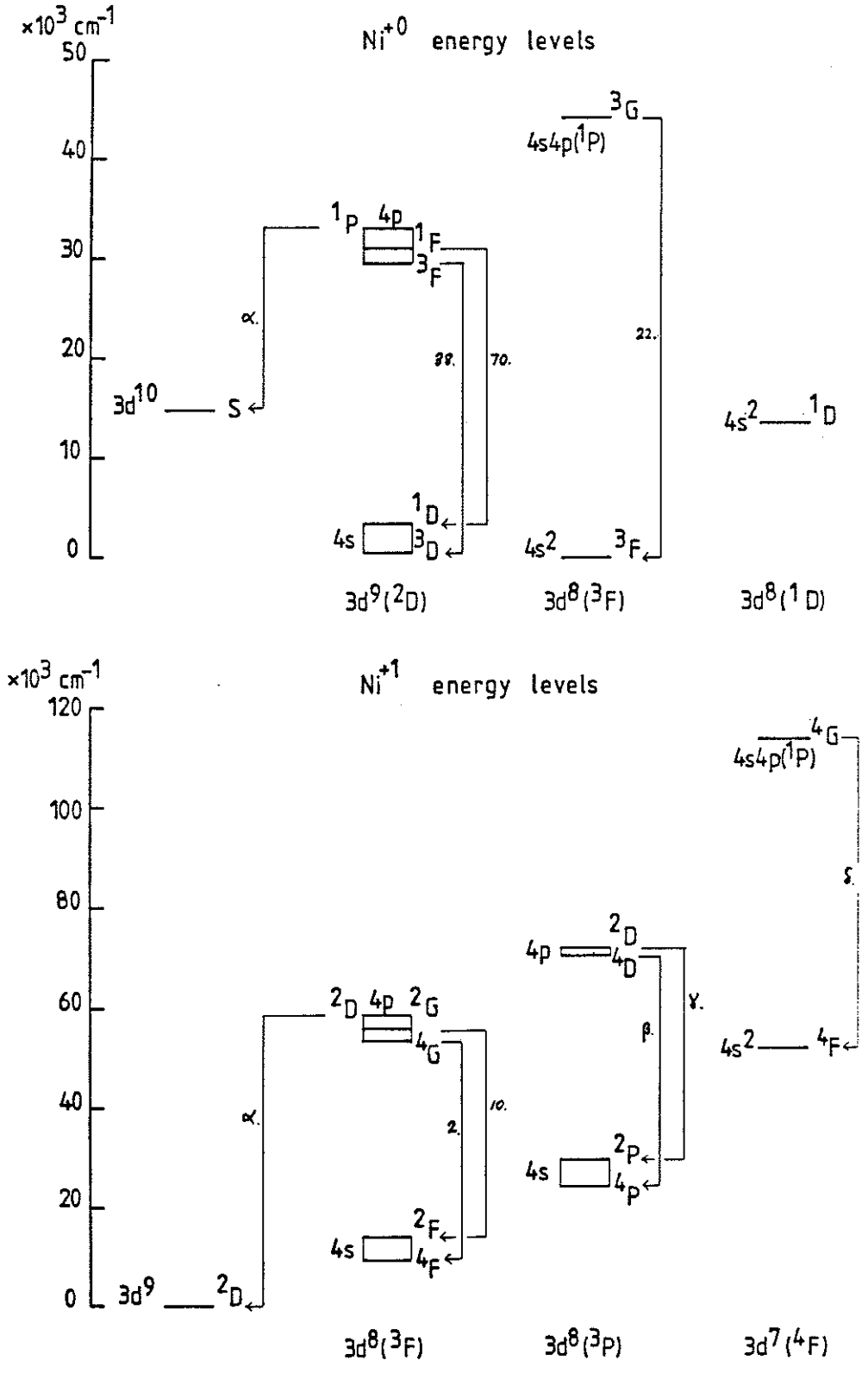

Fig. 9a & 9b Energy levels and principal radiative transitions of Ni^{+0} and Ni^{+1}.

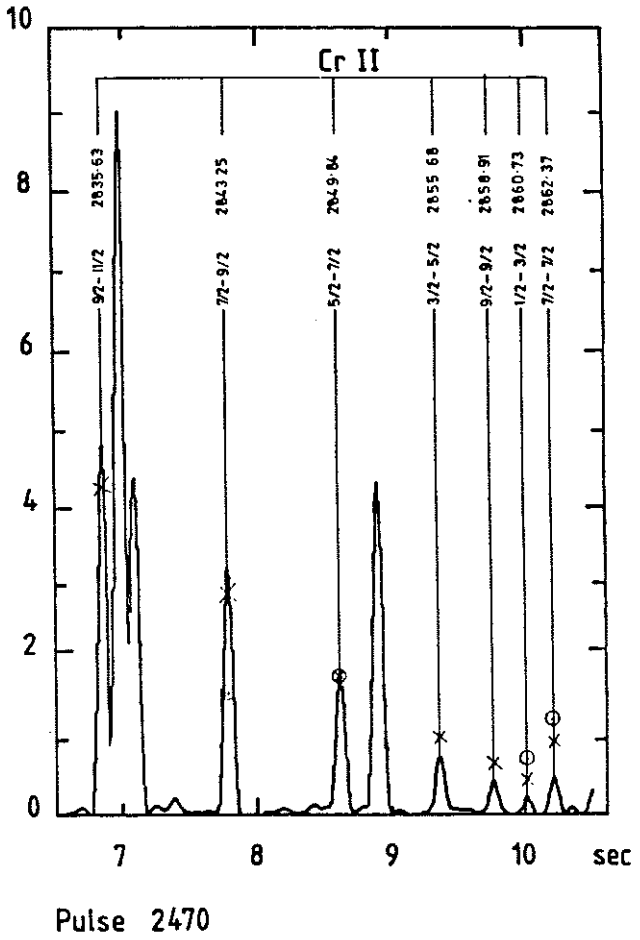

Fig. 10 JET limiter spectrum showing Cr^{+1} multiplet 1 components. *X*, White-Eliason (1933) relative strengths; *O*, Younger et al (1978) relative strengths, normalised to 5/2-7/2 component.

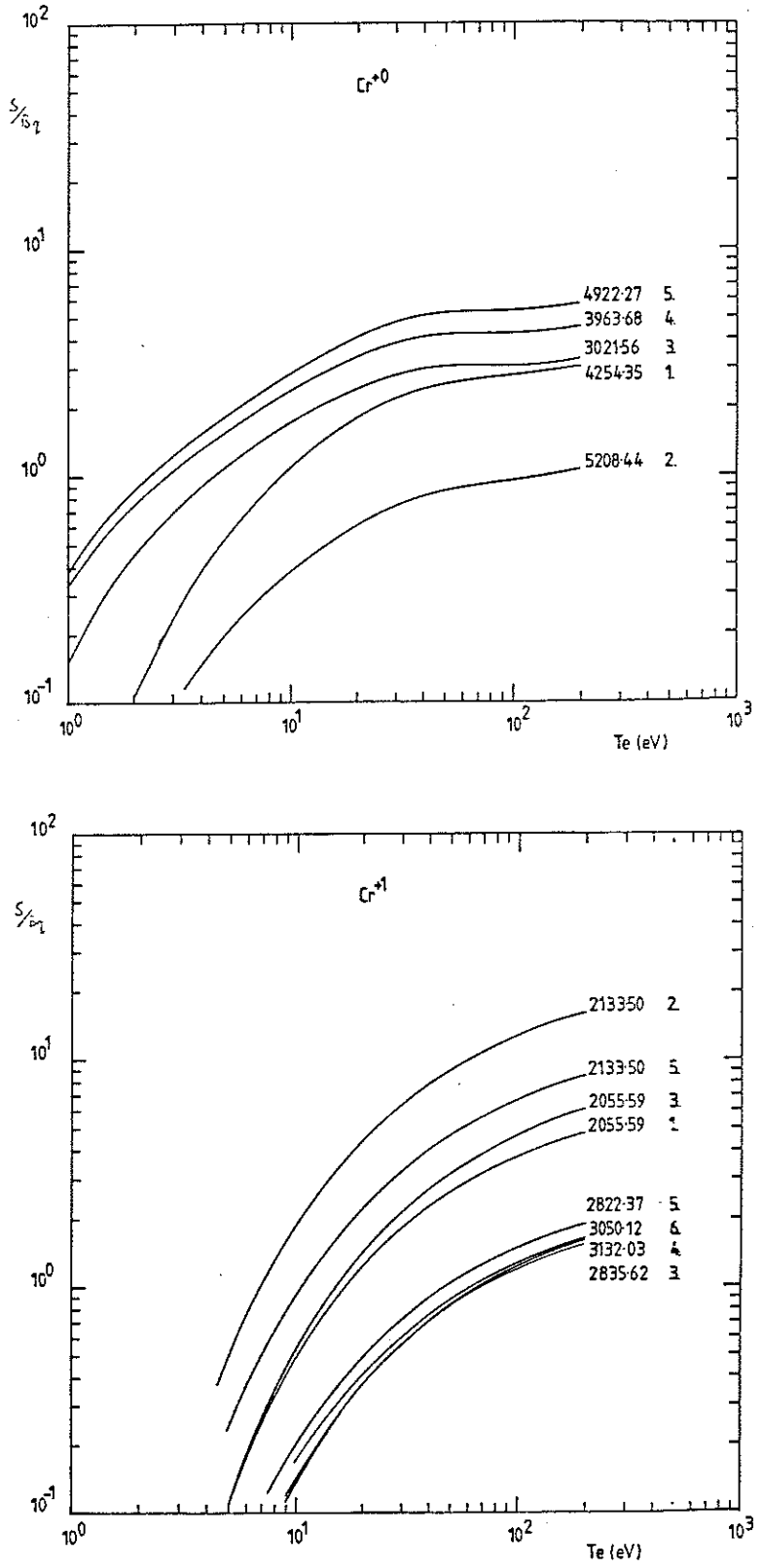

Fig. 11a & 11b Ionisations/photon at zero density for Cr^{+0} and Cr^{+1}. (Curves are labelled by wavelength and metastable index, see Tables 4a, 4b. *B* is the branching ratio, see equation 12).

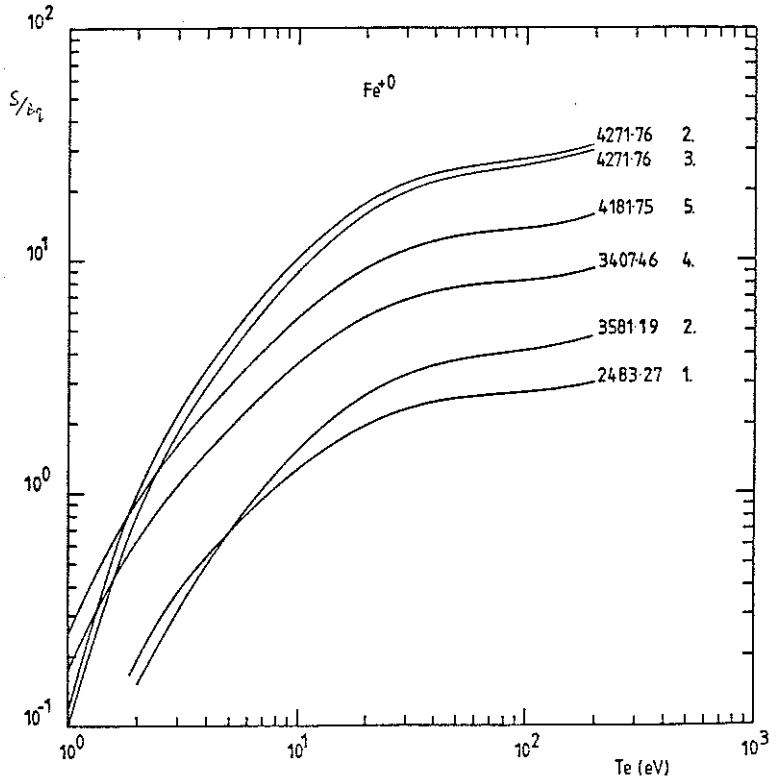

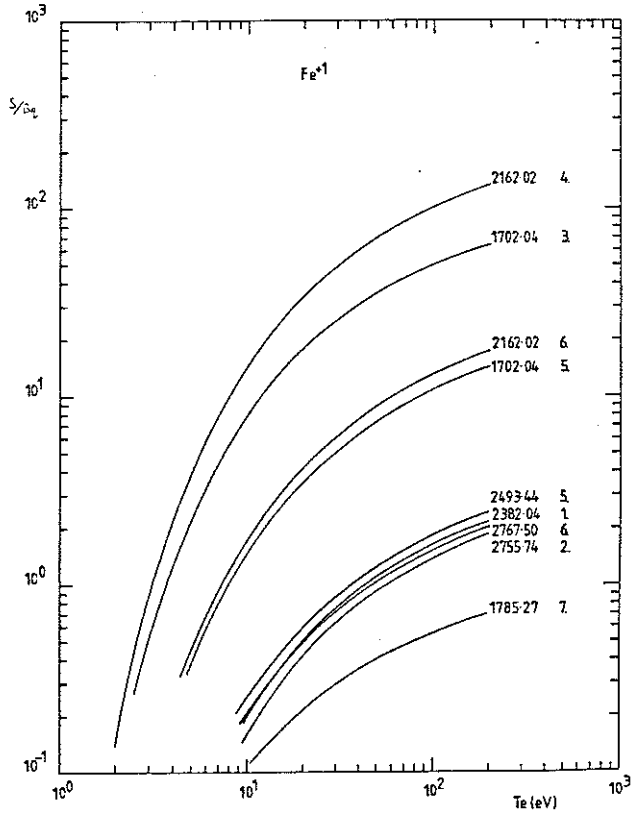

Fig. 12a & 12b Ionisation/photon at zero density for Fe^{+0} and Fe^{+1}.

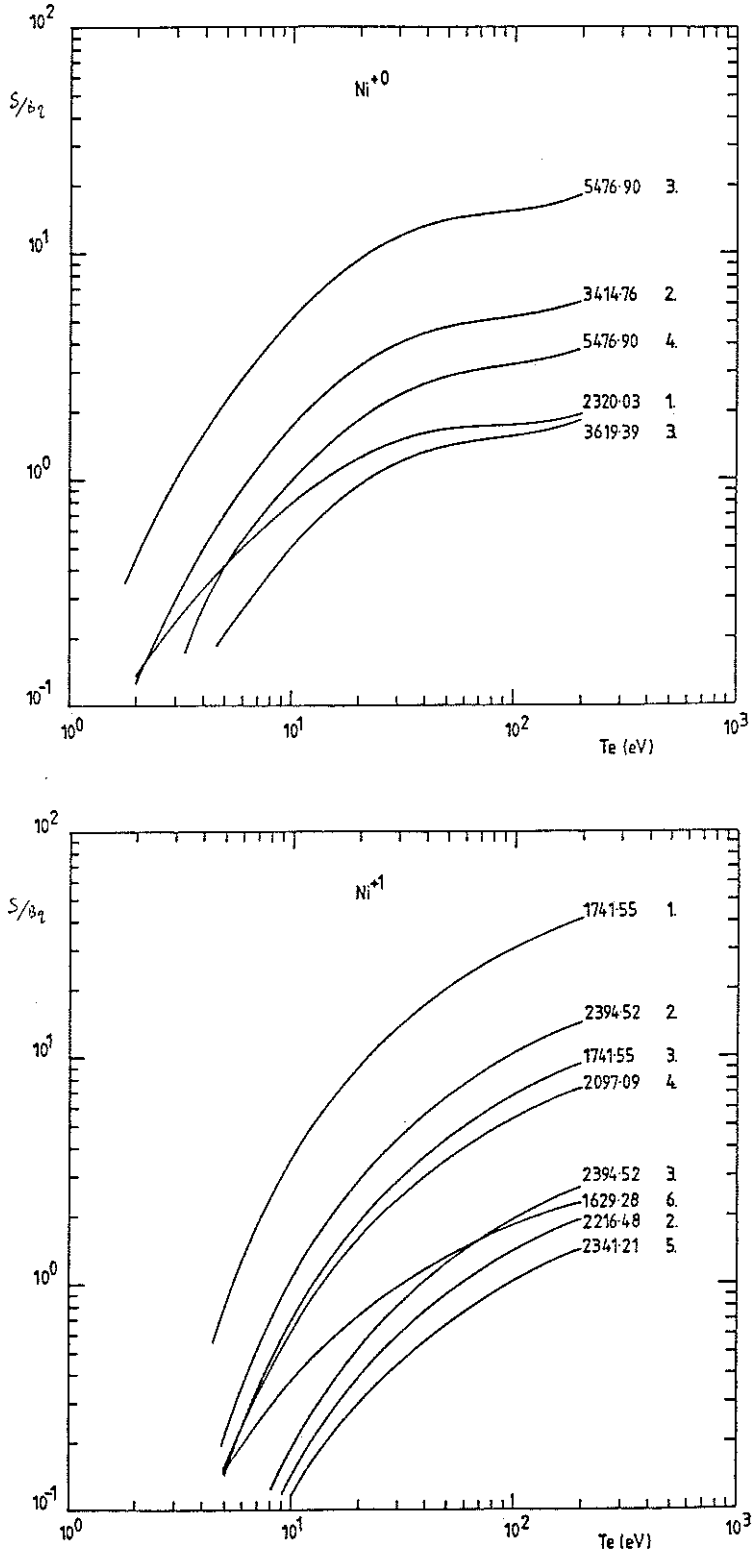

Fig. 13a & 13b Ionisations/photon at zero density for Ni^{+0} and Ni^{+1}.

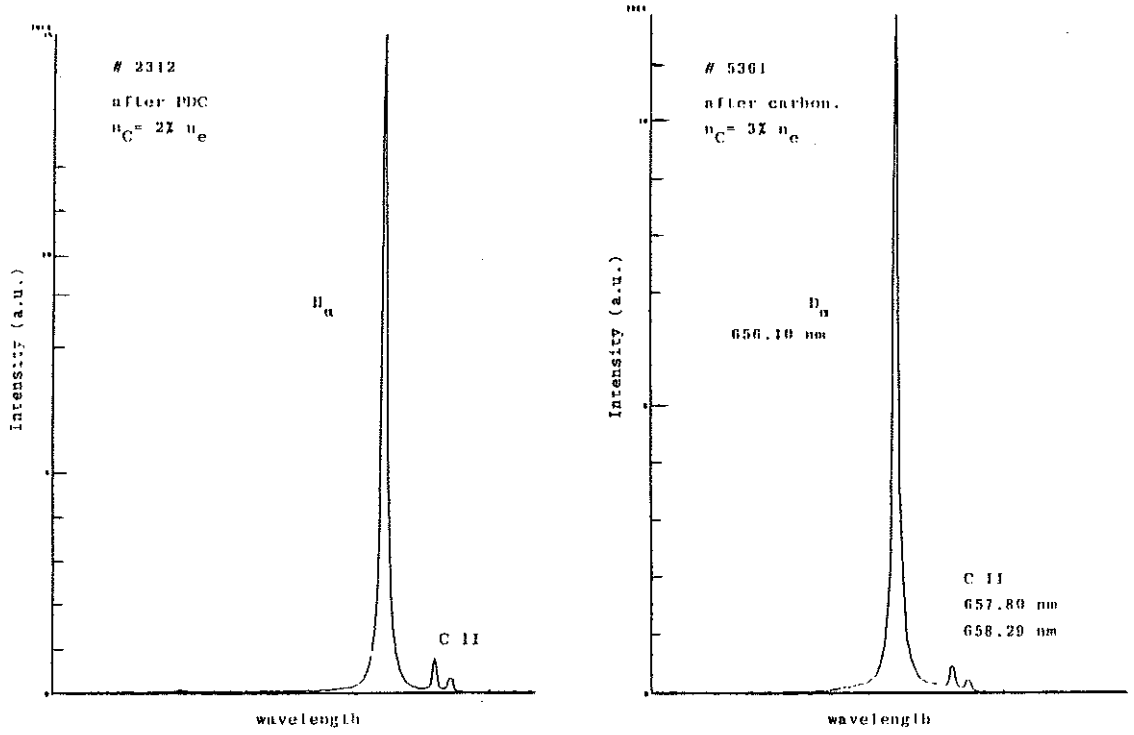

Fig. 14 Recorded spectra in the visible used for deriving carbon limiter fluxes.

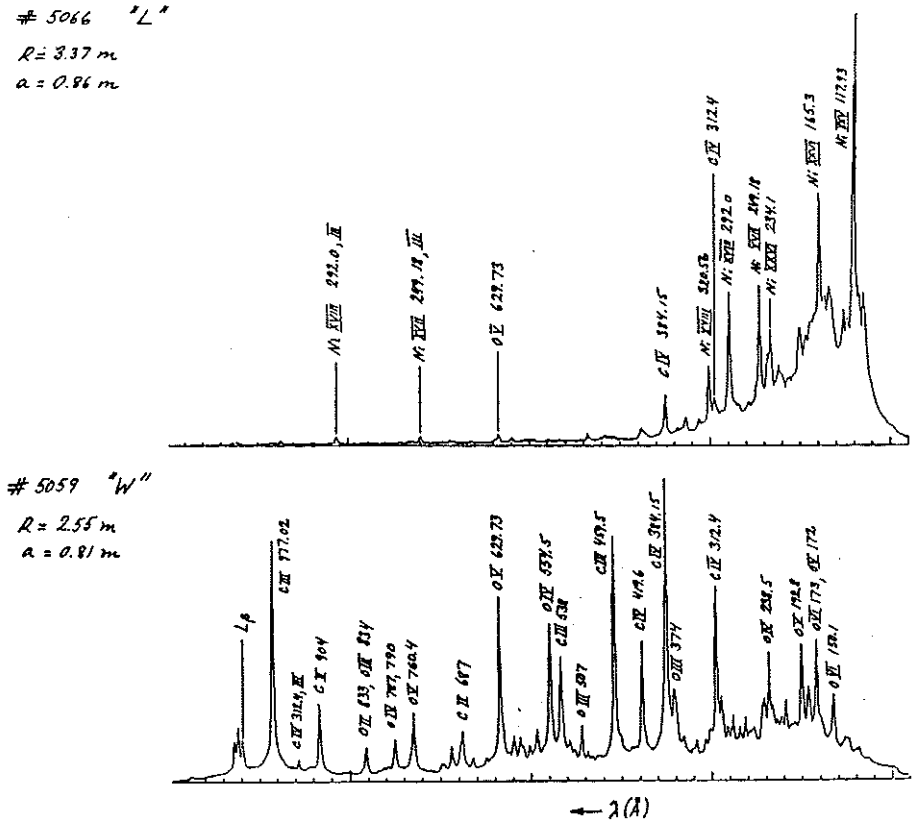

Fig. 15 VUV spectra for small plasmas (a=0.8m) at the carbon limiters ('L') and at the inner wall ('W').

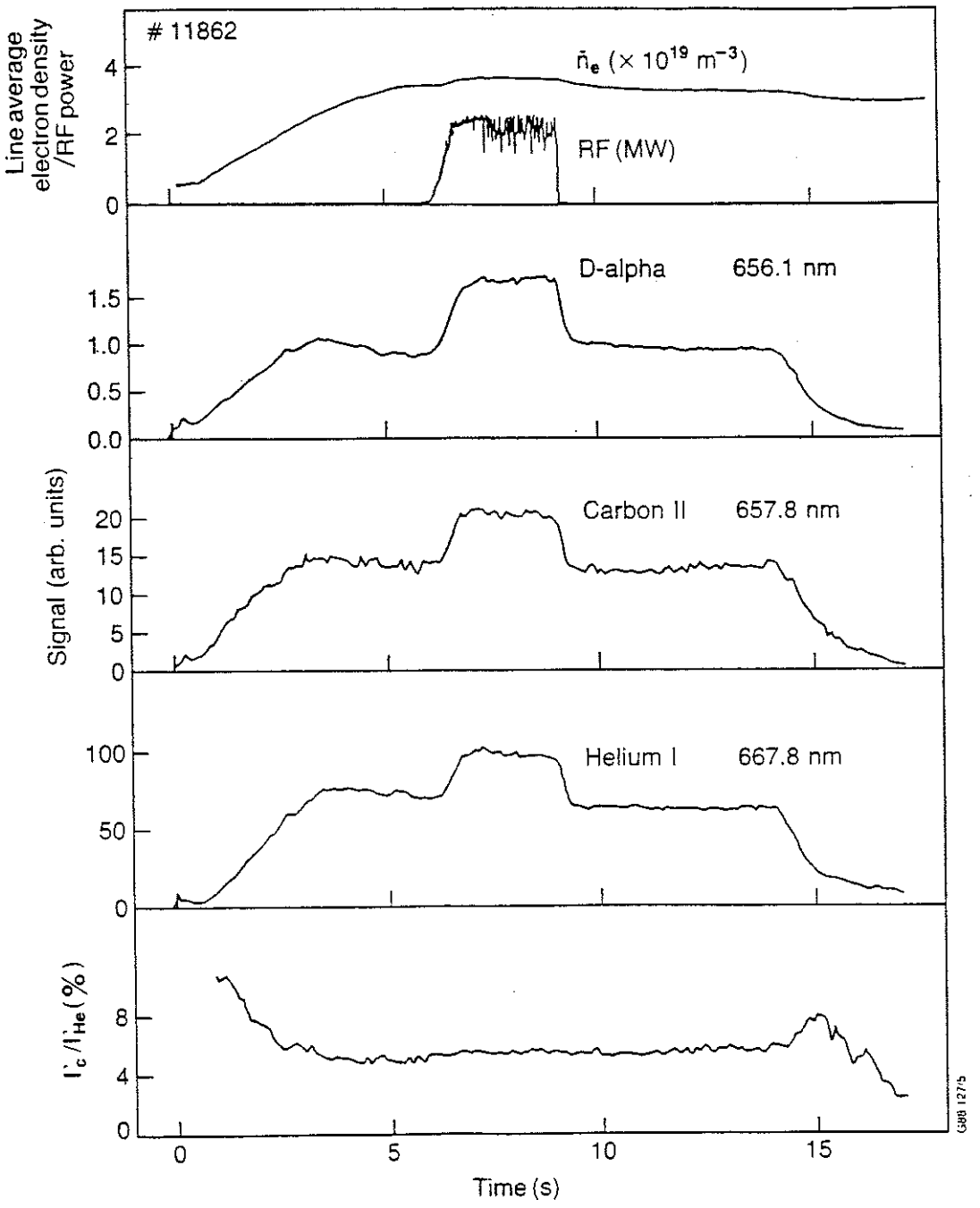

Fig. 16 Parameters of JET pulse #11862.

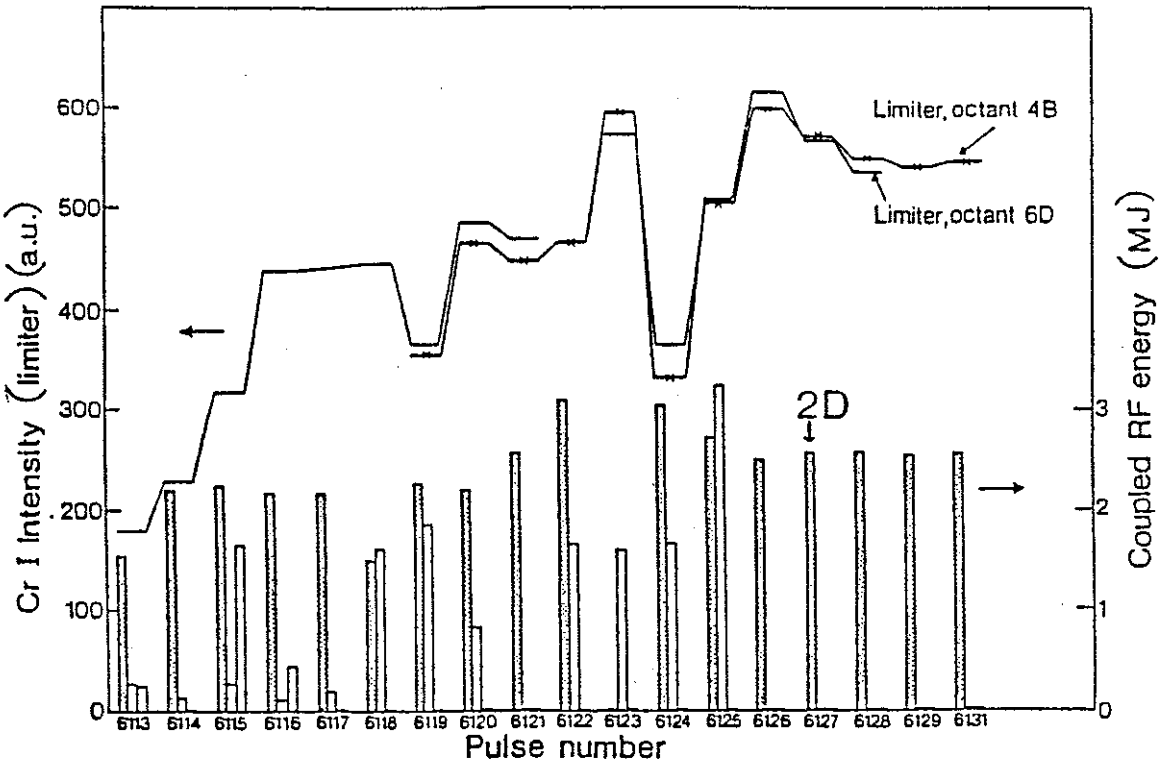

Fig. 17 Cr I line intensity (two limiter views) demonstrating the contamination and cleaning of the limiters as a function of radio frequency heating antenna operation. The 2D antenna (cross hatched) has a chromium coated screen whereas the other antenna (unhatched) have nickel coated screens. The Cr I signal is measured before antenna operation for each pulse.

APPENDIX 1.

THE JET TEAM

JET Joint Undertaking, Abingdon, Oxon, OX14 3EA, U.K.

J.M.Adams[1], F.Alladio[4], H.Altmann, R.J.Anderson, G.Appruzzese, W.Bailey, B.Balet, D.V.Bartlett, L.R.Baylor[24], K.Behringer, A.C.Bell, P.Bertoldi, E.Bertolini, V.Bhatnagar, R.J.Bickerton, A.Boileau[3], T.Bonicelli, S.J.Booth, G.Bosia, M.Botman, D.Boyd[31], H.Brelen, H.Brinkschulte, M.Brusati, T.Budd, M.Bures, T.Businaro[4], H.Buttgereit, D.Cacaut, C.Caldwell-Nichols, D.J.Campbell, P.Card, J.Carwardine, G.Celentano, P.Chabert[27], C.D.Challis, A.Cheetham, J.Christiansen, C.Christodoulopoulos, P.Chuilon, R.Claesen, S.Clement[30], J.P.Coad, P.Colestock[6], S.Conroy[13], M.Cooke, S.Cooper, J.G.Cordey, W.Core, S.Corti, A.E.Costley, G.Cottrell, M.Cox[7], P.Cripwell[13], F.Crisanti[4], D.Cross, H.de Blank[16], J.de Haas[16], L.de Kock, E.Deksnis, G.B.Denne, G.Deschamps, G.Devillars, K.J.Dietz, J.Dobbing, S.E.Dorling, P.G.Doyle, D.F.Düchs, H.Duquenoy, A.Edwards, J.Ehrenberg[14], T.Elevant[12], W.Engelhardt, S.K.Erents[7], L.G.Eriksonn[5], M.Evrard[2], H.Falter, D.Flory, M.Forrest[7], C.Froger, K.Fullard, M.Gadeberg[11], A.Galetsas, R.Galvao[8], A.Gibson, R.D.Gill, A.Gondhalekar, C.Gordon, G.Gorini, C.Gormezano, N.A.Gottardi, C.Gowers, B.J.Green, F.S.Griph, M.Gryzinski[26], R.Haange, G.Hammett[6], W.Han[9], C.J.Hancock, P.J.Harbour, N.C.Hawkes[7], P.Haynes[7], T.Hellsten, J.L.Hemmerich, R.Hemsworth, R.F.Herzog, K.Hirsch[14], J.Hoekzema, W.A.Houlberg[24], J.How, M.Huart, A.Hubbard, T.P.Hughes[32], M.Hugon, M.Huguet, J.Jacquinot, O.N.Jarvis, T.C.Jernigan[24], E.Joffrin, E.M.Jones, L.P.D.F.Jones, T.T.C.Jones, J.Källne, A.Kaye, B.E.Keen, M.Keilhacker, G.J.Kelly, A.Khare[15], S.Knowlton, A.Konstantellos, M.Kovanen[21], P.Kupschus, P.Lallia, J.R.Last, L.Lauro-Taroni, M.Laux[33], K.Lawson[7], E.Lazzaro, M.Lennholm, X.Litaudon, P.Lomas, M.Lorentz-Gottardi[2], C.Lowry, G.Magyar, D.Maisonnier, M.Malacarne, V.Marchese, P.Massmann, L.McCarthy[28], G.McCracken[7], P.Mendonca, P.Meriguet, P.Micozzi[4], S.F.Mills, P.Millward, S.L.Milora[24], A.Moissonnier, P.L.Mondino, D.Moreau[17], P.Morgan, H.Morsi[14], G.Murphy, M.F.Nave, M.Newman, L.Nickesson, P.Nielsen, P.Noll, W.Obert, D.O'Brien, J.O'Rourke, M.G.Pacco-Düchs, M.Pain, S.Papastergiou, D.Pasini[20], M.Paume[27], N.Peacock[7], D.Pearson[13], F.Pegoraro, M.Pick, S.Pitcher[7], J.Plancoulaine, J-P.Poffé, F.Porcelli, R.Prentice, T.Raimondi, J.Ramette[17], J.M.Rax[27], C.Raymond, P-H.Rebut, J.Removille, F.Rimini, D.Robinson[7], A.Rolfe, R.T.Ross, L.Rossi, G.Rupprecht[14], R.Rushton, P.Rutter, H.C.Sack, G.Sadler, N.Salmon[13], H.Salzmann[14], A.Santagiustina, D.Schissel[25], P.H.Schild, M.Schmid, G.Schmidt[6], R.L.Shaw, A.Sibley, R.Simonini, J.Sips[16], P.Smeulders, J.Snipes, S.Sommers, L.Sonnerup, K.Sonnenberg, M.Stamp, P.Stangeby[19], D.Start, C.A.Steed, D.Stork, P.E.Stott, T.E.Stringer, D.Stubberfield, T.Sugie[18], D.Summers, H.Summers[20], J.Taboda-Duarte[22], J.Tagle[30], H.Tamnen, A.Tanga, A.Taroni, C.Tebaldi[23], A.Tesini, P.R.Thomas, E.Thompson, K.Thomsen[11], P.Trevalion, M.Tschudin, B.Tubbing, K.Uchino[29], E.Usselmann, H.van der Beken, M.von Hellermann, T.Wade, C.Walker, B.A.Wallander, M.Walravens, K.Walter, D.Ward, M.L.Watkins, J.Wesson, D.H.Wheeler, J.Wilks, U.Willen[12], D.Wilson, T.Winkel, C.Woodward, M.Wykes, I.D.Young, L.Zannelli, M.Zarnstorff[6], D.Zasche[14], J.W.Zwart.

PERMANENT ADDRESS

1. UKAEA, Harwell, Oxon. UK.
2. EUR-EB Association, LPP-ERM/KMS, B-1040 Brussels, Belgium.
3. Institute National des Récherches Scientifique, Quebec, Canada.
4. ENEA-CENTRO Di Frascati, I-00044 Frascati, Roma, Italy.
5. Chalmers University of Technology, Göteborg, Sweden.
6. Princeton Plasma Physics Laboratory, New Jersey, USA.
7. UKAEA Culham Laboratory, Abingdon, Oxon. UK.
8. Plasma Physics Laboratory, Space Research Institute, Sao José dos Campos, Brazil.
9. Institute of Mathematics, University of Oxford, UK.
10. CRPP/EPFL, 21 Avenue des Bains, CH-1007 Lausanne, Switzerland.
11. Risø National Laboratory, DK-4000 Roskilde, Denmark.
12. Swedish Energy Research Commission, S-10072 Stockholm, Sweden.
13. Imperial College of Science and Technology, University of London, UK.
14. Max Planck Institut für Plasmaphysik, D-8046 Garching bei München, FRG.
15. Institute for Plasma Research, Gandhinagar Bhat Gujat, India.
16. FOM Instituut voor Plasmafysica, 3430 Be Nieuwegein, The Netherlands.
17. Commissiariat à L'Energie Atomique, F-92260 Fontenay-aux-Roses, France.
18. JAERI, Tokai Research Establishment, Tokai-Mura, Naka-Gun, Japan.
19. Institute for Aerospace Studies, University of Toronto, Downsview, Ontario, Canada.
20. University of Strathclyde, Glasgow, G4 ONG, U.K.
21. Nuclear Engineering Laboratory, Lapeenranta University, Finland.
22. JNICT, Lisboa, Portugal.
23. Department of Mathematics, Univeristy of Bologna, Italy.
24. Oak Ridge National Laboratory, Oak Ridge, Tenn., USA.
25. G.A. Technologies, San Diego, California, USA.
26. Institute for Nuclear Studies, Swierk, Poland.
27. Commissiariat à l'Energie Atomique, Cadarache, France.
28. School of Physical Sciences, Flinders University of South Australia, South Australia SO42.
29. Kyushi University, Kasagu Fukuoka, Japan.
30. Centro de Investigaciones Energeticas Medioambientales y Techalogicas, Spain.
31. University of Maryland, College Park, Maryland, USA.
32. University of Essex, Colchester, UK.
33. Akademie de Wissenschaften, Berlin, DDR.

CR 88.49.1A